Effect of Fluoroethylene Carbonate on the Electrochemical Battery Performance and Surface Film Formation Mechanism of Amorphous MoO$_2$ Lithium-Ion Secondary Battery Negative Electrodes

리튬이온 이차전지 비정질 MoO$_2$ 음극의 전기화학적 전지 성능 및 표면피막 형성 메커니즘에 미치는 Fluoroethylene Carbonate 효과

2014년 2월

서울대학교 대학원

화학생물공학부

박 종 우

Effect of Fluoroethylene Carbonate on the Electrochemical Battery Performance and Surface Film Formation Mechanism of Amorphous MoO$_2$ Lithium-Ion Secondary Battery Negative Electrodes

리튬이온 이차전지 비정질 MoO$_2$ 음극의 전기화학적 전지 성능 및 표면피막 형성 메커니즘에 미치는 Fluoroethylene Carbonate 효과

지도교수 김 재 정

이 논문을 공학석사 학위 논문으로 제출함

2013년 10월

서울대학교 대학원

화학생물공학부

박 종 우

박종우의 석사 학위 논문을 인준함

2013년 12월

위 원 장 ＿＿＿＿＿＿＿＿(인)

부위원장 ＿＿＿＿＿＿＿＿(인)

위 　 원 ＿＿＿＿＿＿＿＿(인)

Abstract

Effect of Fluoroethylene Carbonate on the Electrochemical Battery Performance and Surface Film Formation Mechanism of Amorphous MoO$_2$ Lithium-Ion Secondary Battery Negative Electrodes

Jongwoo Park

School of Chemical and Biological Engineering

The Graduate School

Seoul National University

Lithium-ion secondary batteries (LIBs) are the most promising electrochemical devices for energy storage system based on their superior energy storage performance. In spite of their success, many intensive works have consistently been devoted to improve capacity, energy and power density of LIBs by developing new electrode materials and controlling stable interphase. Among the various electrode material candidates, molybdenum dioxide (MoO$_2$) has been reviewed as one of negative electrode materials due to its attractive properties such as fairly low electrical resistivity, high thermal and chemical stability. However, similar to other electrode materials, solid electrolyte

i

interphase (SEI) is also formed on MoO_2 electrode surface after repetitive galvanostatic cycling. SEI formation is responsible for prolonged cycleability since it is an inevitable side reaction that leads to battery performance degradation. Hence well characterization and control of the highly ion conductive, mechanically and electrochemically stable, and thin SEIs are also required for MoO_2-based LIBs.

In this research, the positive impact of fluoroethylene carbonate (FEC), a typical SEI former additive, on the electrochemical battery performance and SEI formation mechanism of nano-sized amorphous molybdenum dioxide (a-MoO_2) was investigated. The various contents of FEC were combined in the electrolyte as an alternative co-solvent to identify different SEI formation mechanism which can explain the electrochemical behavior of a-MoO_2 electrodes. The capacity retention was enhanced as a function of FEC concentration up to approximately 7% after 50 cycles. To explain the electrochemical performance of a-MoO_2 in FEC-containing system, the surface chemistry was characterized by using electrochemical impedance spectroscopy (EIS), field emission-scanning electron microscope (FE-SEM), Fourier transform-infrared spectroscopy (FT-IR), and X-ray photoelectron spectroscopy (XPS). As a result of successive reductive decomposition of FEC on the electrode surface, a highly ion conductive, mechanically and electrochemically stable, and thin SEI was developed. It originated from FEC-reduced products that are rich in polycarbonates and LiF. Based on the findings, we identified the properties of the surface films and developed their formation mechanism with and without FEC for ethylene carbonate (EC)-derived, FEC-derived, and EC-/FEC-co-derived SEI, respectively. The identification of SEI formation mechanism proposed herein might provide a good idea in understanding the effect of

FEC as an effectual alternative co-solvent for modifying the surface chemistry of typical LIB negative electrodes. To the best of our knowledge, this is the first report on identifying surface chemistry mechanism of a-MoO$_2$ negative electrode with FEC.

Key words: lithium-ion secondary batteries; amorphous molybdenum dioxide; solid electrolyte interphase; fluoroethylene carbonate; surface chemistry.

Contents

List of Tables

List of Figures

1. Introduction

1.1. Fundamentals of Energy Storage

A rapid development in the energy industry involved a new era of alternetive energy sources and effective energy storage system. As the environmental challenge of global warming resulted from the consumption of fossil fuel is growing more severe, the importance of electrochemical energy conversion and storage devices for sustainable and eco-friendly alternative energy and power sources is emphasized more than ever. To break away from traditional energy generation methods and realize an eco-friendly energy industry, it has become very important issue to establish a totally new energy conversion and storage technology.

Richard E. Smalley expected that renewable energy sources, e.g. solar, wind, and geothermal energy, will take up 50% of total energy supply by year of 2050.[1] This energy conversion issue cannot separately be discussed from energy storage method. Because such alternative energy sources are sustainable but not continuous in everyday life, it is essential to provide well-developed energy storage system to retain all the advantages of renewable energy. Such a world's energy breakdown requires new era of advanced lithium-ion secondary batteris and/or other kinds of energy storage devices.

Lithium-ion secondary batteries, supercapacitors, fuel cells and other kinds of secondary batteris are the typical electrochemical devices for energy storage system. In Table 1.1, the various types of present and future secondary or rechargeable batteris and

their chemistries are listed. A variety of storage devices had developed their features and performance accompanied with environmental impacts. There are many alternative candidates of future battery system including sodium-ion, lithium-air, and lithium-orgnic batteries. The trend of future battery system reflects academic and industrial efforts toward the improvement in electrochemical battery performance, extension in applications, as well as the environmental issues in materials and industry processes. However, as shown in the table, despite of the several challenges facing lithium chemistry, lithium-ion secondary batteries are the most promising system among the established ones up to now.

Lithium-ion secondary batteries had received a great attention due to their high specific capacity (3860 mAh/g) and energy density resulting from low atomic weight and the lowest standard electrode potential (-3.04 V *vs*. NHE) of lithium. Therefore the lithium-ion secondary batteries are comparatively small and light compared to other storage devices or secondary batteries.[62] Moreover they are relatively free in diversity of active materials and regulation on the size of batteries. Along with these features, lithium-ion secondary batteries became the most promising electrochemical device that can satisfy the requirements of high energy and power capability. Nowadays lithium-ion secondary batteries are extending their applications in portable electronic devices, electric vehicles, implantable medical devices, building integration, and so forth[2] as represented in Figure 1.1. In spite of the success of lithium-ion secondary batteries in the energy storage market, many intensive works have continuously been devoted to overcome critical challenges; high capacity electrode materials, new electrolyte materials, enhanced energy and power density, and quality of interfaces at the electrode surface.

2

Table 1.1. The Various Types of Present and Future Secondary Batteries, and Their Chemistries[21]

Battery type	Features	Environmental impact
Ni–MH (established)	Low voltage, moderate energy density, high power density Applications: portable, large-scale	Nickel not green (difficult extraction/unsustainable), toxic. Not rare but limited Recyclable
Lead–acid (established)	Poor energy density, moderate power rate, low cost Applications: large-scale, start-up power, stationary	High-temperature cyclability limited Lead is toxic but recycling is efficient to 95%
Lithium ion (established)	High energy density, power rate, cycle life, costly Applications: portable, possibly large-scale	Depletable elements (cobalt) in most applications; replacements manganese and iron are green (abundant and sustainable) Lithium chemistry relatively green (abundant but the chemistry needs to be improved) Recycling feasible but at an extra energy cost
Zinc–air (established)	Medium energy density, high power density Applications: large-scale	Mostly primary or mechanically rechargeable Zinc smelting not green, especially if primary Easily recyclable
Lithium–organic (future)	High capacity and energy density but limited power rate. Technology amenable to a low cost Applications: medium- and large-scale, with the exception of power tools	Rechargeable Excellent carbon footprint Renewable electrodes Easy recycling
Lithium–air (future)	High energy density but poor energy efficiency and rate capability Technology amenable to a low cost Applications: large-scale, preferably stationary	Rechargeability to be proven Excellent carbon footprint Renewable electrodes Easy recycling
Magnesium–sulphur (future)	Predicted: high energy density, power density unknown, cycle life unknown	Magnesium and sulphur are green Recyclable Small carbon footprint
Al–CF$_x$ (future)	Predicted: moderate energy density, power density unknown	Aluminium and fluorine are green but industries are not Recyclable
Proton battery (future)	Predicted: all organic, low voltage, moderate energy density, power density unknown	Green, biodegradable
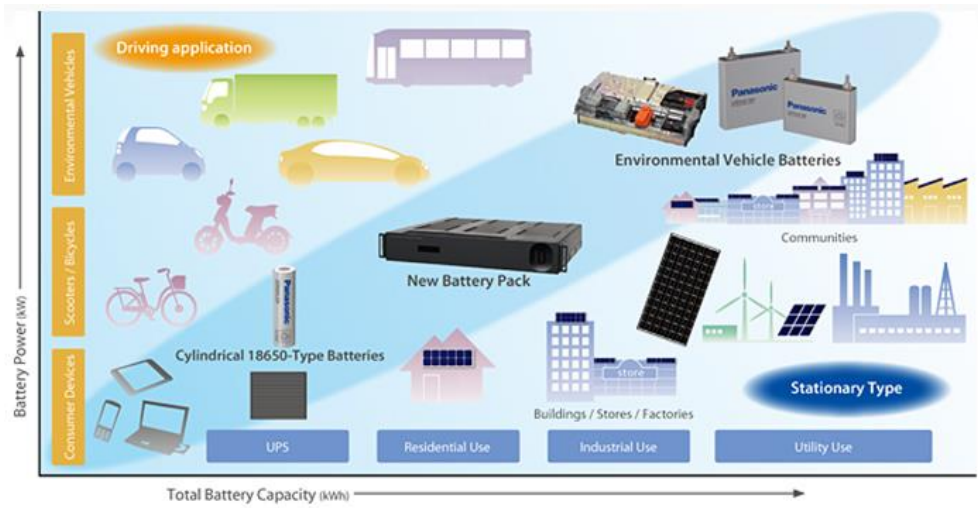
Figure 1.1. Various application fields of lithium-ion secondary batteries. Excerpted from the website of Panasonic, *Panasonic's Battery Business*.

1.2. Lithium-Ion Secondary Batteries

As the electronics become miniaturized, the batteries of small size and long-term stability are required as well as the energy and power density, safety, reliability, and cost issues. Based on their simple operating system accompanied with superior performance to the other competitors, lithium-ion secondary batteries have been adopted as major power sources in recent studies.

1.2.1. Lithium-Ion Secondary Battery System

Figure 1.2(a) exhibits the fundamental operating system of the lithium-ion secondary batteries. An external electrical energy is provided into the cell during charge process. Lithium ions are extracted from the positive electrode and transferred to the negative electrode through the electrolyte. At the end, lithium ions combine with electrons in the negative electrode, and hence are stored as lithium atoms. An exact reverse reaction occurs during spontaneous and galvanostatic discharge process.

The commercialized insertion type positive and negative electrodes are $LiCoO_2$ and graphite, respectively. In discharge process, the negative electrode undergoes anodic reaction and positive electrode follows cathodic reaction. The following equations describe chemical reactions that occur while charge/discharge process at each electrode.

Discharge: Positive electrode; $2Li_{0.5}CoO_2 + Li^+ + e^- \rightarrow 2LiCoO_2$ (reduction)

$$\text{Negative electrode; LiC}_6 \;\rightarrow\; 6C + Li^+ + e^- \;\text{(oxidation)}$$

$$\textit{Charge}: \text{Positive electrode; } 2LiCoO_2 \;\rightarrow\; 2Li_{0.5}CoO_2 + Li^+ + e^- \;\text{(oxidation)}$$

$$\text{Negative electrode; } 6C + Li^+ + e^- \;\rightarrow\; LiC_6 \;\text{(reduction)}$$

According to the above reactions, the extracted lithium ions from negative electrode move toward positive electrode while discharging, and *vice versa* while charging. Such behavior of lithium ions in battery system is so called rocking chair mechanism.[59] Since the ions are extracted from and inserted into the host electrode materials, there are no accumulations resulting from battery reaction. Moreover the active materials and electrolyte are retained throughout the entire cycling because the main operating mechanism only involves lithium ion transportation. De-/intercalation of lithium ions from and into the host materials can generally be classified into three groups; insertion reaction, alloying reaction, and conversion reaction. Each mechanism requires different lithium chemistry and results in different electrochemical behaviors of battery.

The current researches focus not only on the individual components but also on the total system of batteries. One of the most interested phenomena in the system is the quality of interfaces, e.g. electrode and electrolyte. This interfacial issue or the formation of surface film so called solid electrolyte interphase (SEI) will be reviewed further in this paper.

1.2.2. Lithium-Ion Secondary Battery Components

Commonly, the lithium-ion secondary batteries are composed of the negative electrode (or anode), positive electrode (or cathode), electrolyte, and the separator as schematically illustrated in Figure 1.2(b). For a superior electrochemical performance of the batteries, each component must serve sufficient roles and be in harmony. The commercialized major active materials for negative and positive electrode are graphite and $LiCo_{1-x}M_xO_2$ substituted by other atoms in position of M, respectively. Figure 1.3 briefly summarizes a variety of positive and negative electrode materials along with their specific capacity and working voltage. A fundamental review in the working principles and types of electrode materials, and the electrolyte is employed in this chapter.

1.2.2.1. Positive Electrode Materials

Positive electrodes serve as cathodes for discharge process, which implies that lithium ion insertion or lithium ion reduction occurs at the surface. They can roughly be categorized into lithium-free and lithium-containing compounds. Mostly, these materials have tunnel or layered structure where lithium is able to move between or de-/intercalated, respectively. Typical examples of positive electrode materials are layered rock salt structure $LiCoO_2$, spinel structure $LiMn_2O_4$, and olivine structure $LiFePO_4$. Positive electrode materials require spaces for lithium ion diffusion inside their structure, and their structural difference critically affects lithium ion diffusion path. The olivine, layered, and spinel structures adapt 1-dimensional, 2-dimensional, and 3-dimensional diffusion pathway, respectively, which may affect the power capability.

7

The use of Li_xCoO_2 as positive electrode materials was suggested for the first time in 1980[60] and commercialized in the practical devices. $LiCoO_2$ has hexagonal layered structure with alternate cobalt and lithium layer. Lithium ions can move between these layers. $LiCoO_2$ has high operating voltage, and thereby obtains stable cycle performance. However, the deposits of cobalt are rare in universe. Moreover the phase transition to monoclinic lattice structure, which is caused by the degree of lithium reaction, leads to structural instability. To overcome such drawbacks, dioxides of the transition metals, e.g. V, Cr, Fe, Ni, are of interest as alternative positive electrode materials.

$LiMn_2O_4$ is a typical example of the spinel structure (AB_2O_4 structure) that has been noticed much due to its facile synthesis and cheap price. During the lithium reaction, spinel structure expands isotropically maintaining the cubic structure. It has more stable structure compared to layered structure which undergoes anisotropic volume expansion as cycle proceeds. In spite of its less volume change, it suffers from Jahn-Teller distortion due to low oxidation state of manganese that leads to limited cycle performance.

$LiFePO_4$, the olivine structure, is regarded as the first positive electrode material with potentially low cost and plentiful elements and also environmental friendliness. $LiFePO_4$ shows no critical capacity fading as well as high capacity compared to other materials. A major drawback is its poor electronic conductivity. This is a general characteristic of material containing the poly-anion such as PO_4^{2-} that leads to severe polarization during discharge. It can be improved by carbon coating, doping with heterogeneous atom, and using nano-sized particles.[61]

1.2.2.2. Negative Electrode Materials

Lithium metal was initially used as negative electrode material for lithium secondary batteries. It could attain high energy density due to the low operating voltage and high specific capacity, but lithium dendrite was formed during repetitive charge/discharge process as a result of inhomogeneous lithium deposition. The lithium dendrite continuously grows and damages the separator, and contact with positive electrode. The internal electrical short leads to risk of ignition or explosion. Thereof in terms of safety issue, lithium metal is replaced by the materials that contain lithium ion or that can react with lithium ions. The de-/intercalation or de-/alloying mechanism of lithium ions governed by rocking chair mechanism had improved safety of the batteries.

Carbon negative electrode materials have been adopted as major material in typical lithium-ion secondary batteries since the first commercialization by SONY in 1990s. Up to now, carbons are used as the typical negative electrode material due to their higher specific charges and more negative redox potentials (0.1 ~ 0.2 V *vs*. Li/Li$^+$) compared to other materials, and their better dimensional stability than lithium alloys. Carbon materials possess superior conductivity and can roughly be classified into various forms, e.g. graphitic, non-graphitic carbons, depending on the heat treatment temperature. Among the several candidates, graphite shows excellent stability under repetitive cycling. However, it has poor theoretical specific capacity, 372 mAh/g.

To increase the specific capacity, lithium alloy materials, e.g. Si, Sn, Ge, Ga, Al, and transition metal oxides, e.g. MoO_2, TiO_2, V_2O_5, had been considered as alternative negative electrode materials. The metallic or semiconducting elements which can alloy with lithium ions over 0 V *vs*. Li/Li$^+$ at room temperature exhibit higher specific capacity

9

compared to graphite up to over 10 times. However, these materials have an intrinsic drawback of severe volume change during repeated charge/discharge, which leads to electrical disconnection, electrode disintegration and following abrupt capacity fading. Nano-sized materials were suggested to reduce the massive volume change. Moreover, the composite with alloy and inactive matrix have been studied to prevent pulverization of particle and to maintain electrical pathway.

To overcome the demerits of lithium alloying materials, the intermetallic compounds or transition metal oxides are also considered as electrode materials. Transition metal oxides can be divided by two categories according to their reaction mechanism; insertion and conversion reaction. These electrodes exhibit lower theoretical specific capacity compared to that of metal electrodes. But the metals of lower reactivity or lithium oxide, which are inactive matrix, serve as buffer material during lithium ion de-/lithiation. They can release the stress that originates from volume expansion. The general demerits of these materials include a large hysteresis between charge and discharge voltage, severe volume change upon cycling, and a large irreversible capacity evolved at the first cycle. These intrinsic drawbacks originate from an incomplete delithiation or oxidation of metal/LiX nanocomposite.

1.2.2.3. Electrolyte

Electrolyte is a medium for lithium ion transport between the positive and negative electrodes. The interfaces between the electrolyte and the two electrodes are the only

locations where electron exchanges can occur, thus generating a steady orientation flow of electrons *via* an external circuit. Hence the electrolyte must simultaneously be an ion conductor and an electronic insulator.

In electrolytes, lithium salt, e.g. $LiPF_6$, $LiClO_4$, $LiAsF_6$, is dissolved in non-aqueous solvent. The fundamental qualifications include wide electrochemical stability window, high boiling point, low freezing point, and thermal stability to remain inert during the lifetime of the device. The most important of requirements for the electrolyte in lithium-ion secondary batteries is its ion conductivity. For the selection of electrolyte solvents, the dielectric constant and viscosity of them must be considered. Carbonate based electrolyte should possess high dielectric constant for easy ionization of lithium salts and proper viscosity for high lithium ion conductivity, respectively. An appropriate combination between the degree of lithium ion dissociation and ease of ion transport can satisfy a fine level of lithium ion transport. The cyclic carbonates, e.g. ethylene carbonate (EC), propylene carbonate (PC), incorporate high dielectric constant and viscosity due to the presence of electron conjugation structure around the carbonate. Whereas the linear carbonates, e.g. diethyl carbonate (DEC), dimethyl carbonate (DMC), exhibit low viscosity and high conductivity due to low bulk hindrance from the atomic structure. However their attached group on linear carbonates cannot serve as electron polarization, and thereby possess low dielectric constant.[26] Based on these facts, the cyclic and linear carbonates are properly mixed to accomplish high dielectric constant and low viscosity, and be used as electrolyte solvent. The organic carbonates and esters applied as electrolyte solvents are listed in Table 1.2.

The properties of electrolyte are responsible for better electrochemical battery

performance; the facilitate formation of surface film on the electrode surface, reduction in irreversible capacity and gas generation for side reaction, protection of cathode materials from dissolution and overcharge, and so forth. Furthermore, for better battery safety, the lower flammability of organic electrolytes, increase in overcharge tolerance, and the termination of battery operation in abuse conditions are necessary.

(a)

(b)
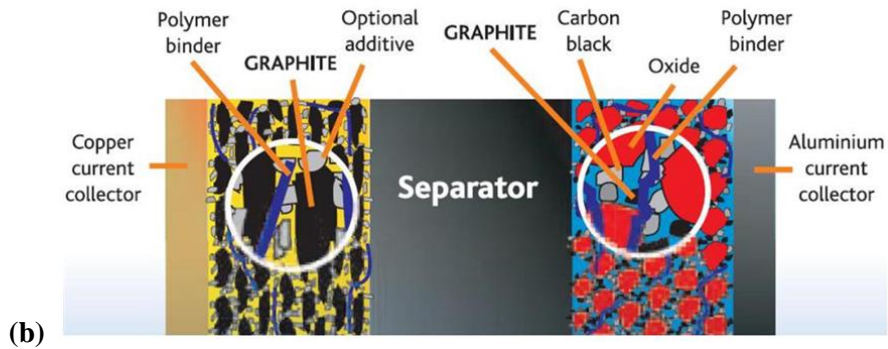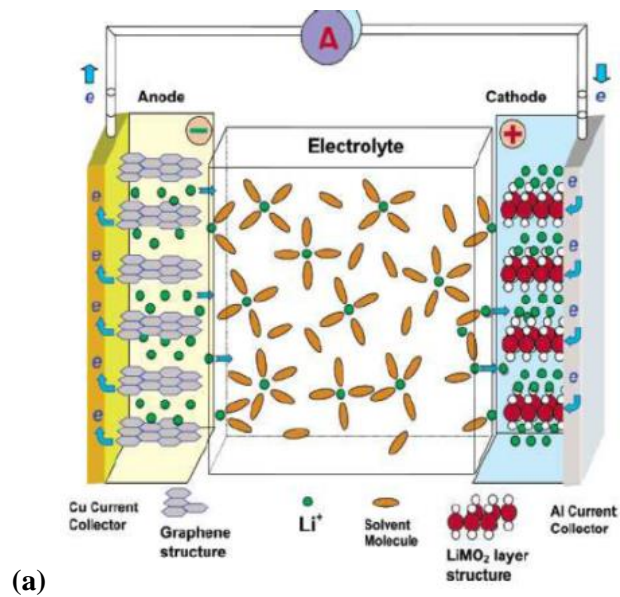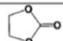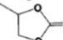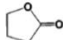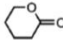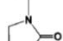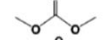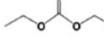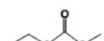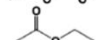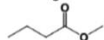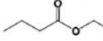
Figure 1.2. (a) The fundamental operating system of lithium-ion secondary batteries[26] and (b) the basic components in the battery system.

1 3
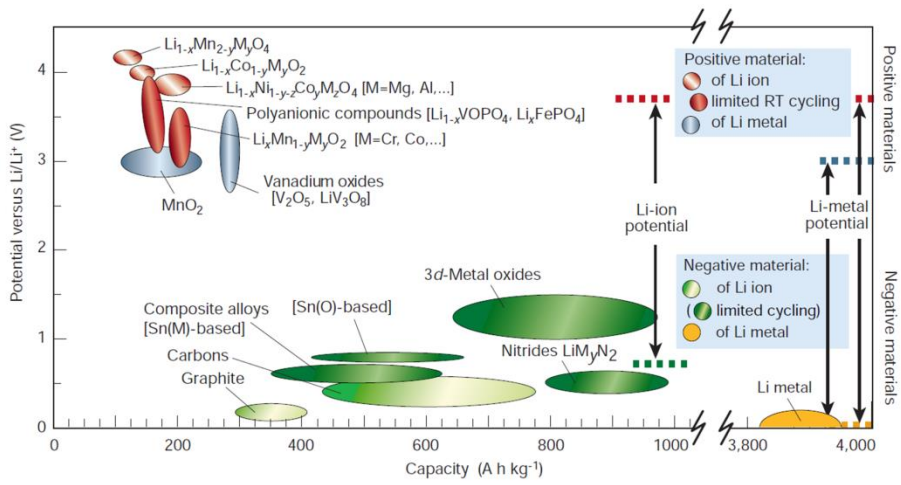
Figure 1.3. Various electrode materials of lithium-ion secondary batteries presently used or seriously considered for the next generation battery systems.[62]

Table 1.2. Organic Carbonates and Esters as Electrolyte Solvents[26]

Solvent	Structure	M. Wt	T_m/ °C	T_b/ °C	η/cP 25 °C	ε 25 °C	Dipole Moment/debye	T_f/ °C	d/gcm⁻³, 25 °C
EC		88	36.4	248	1.90, (40 °C)	89.78	4.61	160	1.321
PC		102	-48.8	242	2.53	64.92	4.81	132	1.200
BC		116	-53	240	3.2	53			
γBL		86	-43.5	204	1.73	39	4.23	97	1.199
γVL		100	-31	208	2.0	34	4.29	81	1.057
NMO		101	15	270	2.5	78	4.52	110	1.17
DMC		90	4.6	91	0.59 (20 °C)	3.107	0.76	18	1.063
DEC		118	-74.3 ᵃ	126	0.75	2.805	0.96	31	0.969
EMC		104	-53	110	0.65	2.958	0.89		1.006
EA		88	-84	77	0.45	6.02		-3	0.902
MB		102	-84	102	0.6			11	0.898
EB		116	-93	120	0.71			19	0.878

1.3. Transition Metal Oxide Negative Electrodes

1.3.1. General Properties of Transition Metal Oxide Materials

Among the wide range of negative electrode materials as already been reviewed in previous chapter, e.g. graphite, Si, Sn, and transition metal oxides, transition metal oxides exhibit competitively high specific capacity and fine mechanical stability of their composite electrodes. Lithium ion intercalation of transition metal oxides is governed by either insertion or conversion reaction as schematically represented in Figure 1.4. Such lithium ion chemistry depends on the degree of native bond strength between metal and oxygen.

Early transition metal (e.g. Ti, V, Cr, Zr, Nb, Mo) oxides undergo insertion reaction with lithium ions at room temperature due to strong bond between transition metal and oxygen. In the case of insertion reaction, lithium ions de-/intercalate from and into the host metal oxide lattice with metal-oxygen bonds maintained. For a long time, numerous insertion or intercalation materials have been proposed as both of positive and negative electrode materials in lithium-ion secondary battery systems. Hence the electrode structure is retained but specific capacity is limited to a certain degree.

On the other hand, late transition metal (e.g. Mn, Fe, Co, Tc, Ru, Rh) oxides can reversibly react with lithium ions by conversion reaction at room temperature due to weak bond between transition metal and oxygen. In the case of conversion reaction, the lattice structure of the host metal oxide is changed due to metal-oxygen bond breaking.

Despite of the possibility of collapse of electrode structure, conversion reaction mechanism guarantees extended capacity based on complete reversible reaction of active material. These materials have attracted much interest owing to the following merits; larger reversible capacity, electrochemically-driven metal/Li_2O nanostructure which enables the re-oxidation of metal, and the possibility of good cycle performance based on the following general equation.[23]

$$MX + nLi^+ + ne^- \rightarrow M + nLiX \text{ (M: transition metal)}$$
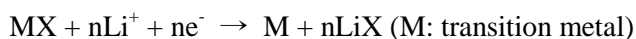
The relevant studies show that a corresponding uptake of lithium ions transforms the transition metal oxide into M/Li_2O nanocomposite in which 2 ~ 5 nm metal grains are embedded in an amorphous Li_2O matrix. Li_2O shows an unusual reactivity at room temperature in such cases. It is contributed to the formation of extremely small separation distances between Li_2O and metal nanograins.[23] It implies that the conversion reaction of transition metal oxides with lithium ions is thermodynamically feasible in non-aqueous electrolyte systems.

Crystallinity of the materials also affects lithium ion chemistry. The crystalline structure exhibits crystallographically restricted lithium ion storage sites, and thereby results in limited specific capacity. On the other hand, the counterpart amorphous structure possesses disordered atomic-scale structure provided with cation vacancies and defects sites that leads to additional lithium ion storage sites inside the active material. Therefore the amorphous structure is preferred to obtain higher theoretical specific capacity.

1.3.2. Molybdenum Dioxide

Molybdenum dioxide (MoO_2) is one of the transition metal oxides that have consistently been reviewed as a negative electrode for lithium-ion batteries. MoO_2 has several attractive properties such as fairly low electrical resistivity, high thermal and chemical stability.[3-9] There have been many trials on the modification of MoO_2 electrode structure (Figure 1.5) to maximize its advantages. However, lithium ion intercalation for MoO_2 is limited to the insertion reaction or one-electron redox reaction at room temperature due to the strong bond between transition metal and oxygen that leads to low specific capacity.[3,5,10] The large activation energy for breaking the bond between metal and oxygen leads to difficulty in realizing conversion reaction for MoO_2 at room temperature.

To overcome such a drawback and extend the lithiation to the conversion reaction, downsizing the material to nano-scale[5,6,11-14] and amorphization of the material[15-20] are considered to be proper approaches. Then the reversible reaction of nano-sized amorphous MoO_2 (a-MoO_2) with lithium ions is governed by the following theoretical four-electron redox conversion reaction at 25°C.[34]

$$MoO_2 + 4Li^+ + 4e^- \leftrightarrow Mo + 2Li_2O \text{ (theoretical specific capacity of 838 mAh/g)}$$

It results from the lowered onset temperature for conversion reaction and extra lithium ion storage sites provided with its structural defects such as vacant sites that significantly

enlarge the specific capacity. In fact, a lattice structure change due to the conversion reaction[21] and a massive volume change of typical transition metal oxides, approximately 100%, have been reported on repetitive cycling which is responsible for electrode degradation.[22,23] In spite of the chance of electrode degradation, its modified lithium chemistry allows large specific capacity along with original merits of a-MoO$_2$ active material.
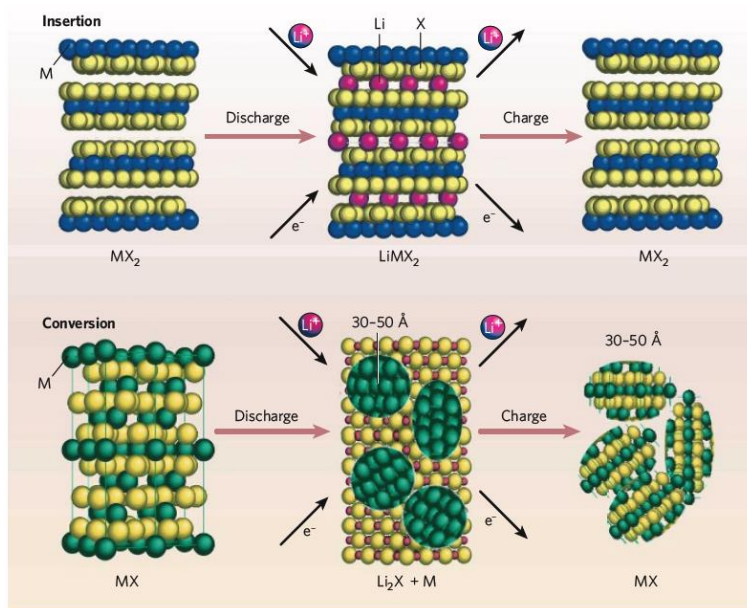
Figure 1.4. Schematic representation of lithium ion reaction mechanisms during charge and discharge process; insertion and conversion reaction. The insertion reaction demonstrates a maximum of one electron transfer per transition metal designated as M, whereas the conversion reaction can transfer 2 to 6 electrons.[21]
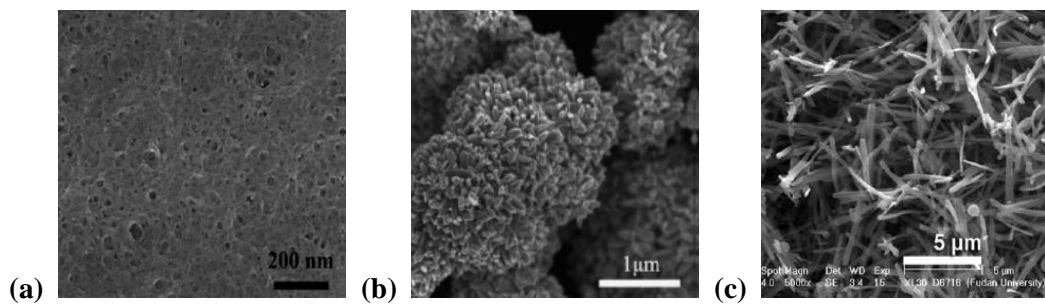
Figure 1.5. Various types of modified structure of MoO_2 electrode; (a) layer-by-layer assembled MoO_2-graphene thin film[33], (b) core-shell MoO_2 hierarchical microcapsule[63], and (c) carbon coated MoO_2 nanobelts[64].

1.4. Solid Electrolyte Interphase

Improving the cycle performance involves stabilizing two critical components of the battery electrodes; the active materials and their interfaces with the electrolyte, SEI. The very first definition of SEI is stated as a passivating layer between an electrode and the electrolyte that arises from the reductive decompositions of a small amount of organic electrolytes by E. Peled. The surface film formation on graphite negative electrodes and their composition have already been thoroughly investigated.[28,56,67] Controlling the SEI formation mechanism accompanied by the surface chemistry modification is an essential step in optimizing the combination of electrode-electrolyte for lithium-ion secondary batteries.

1.4.1. SEI Formation in Battery System

The surface film formation occurs on any form of lithiated negative and positive electrodes due to the fact that the operating potentials of these electrodes are out of electrochemical stability window of electrolyte implying the organic electrolyte solutions are thermodynamically unstable.[24] It results in reduction and oxidation of electrolyte species on negative and positive electrode surface, respectively. A typical illustration of SEI formation mechanism in battery system and the chemical structure of SEI are shown in Figure 1.6. It mainly consists of insoluble reduced solid products such as lithium alkyl carbonates, lithium carbonate, lithium alkoxide, polycarbonates, and ethers[66] as a result

of electrolyte solvent decomposition. These surface films grow to a certain thickness, and serve as an electronic insulator but an ion conductor. Thus lithium ions can be intercalated into the electrode material through the surface film without degrading the host lattice structure.[67]

The surface films are heterogeneously grown throughout the entire cycling even at low rate that can suppress further reaction between the electrolyte species and electrode as well as the surface oxidation of electrodes. On the other hand, since the film formation is a continuous and inevitable side reaction that results in cell degradation with internal impedance rise, capacity and power fading, such a process is an important factor that is responsible for advanced cycleability.[25] Therefore the interphase control must focus on the foundation on which lithium ion chemistry could operate reversibly by satisfying several requirements; high ion conductivity, uniform morphology and chemical composition, good adhesion to electrode surface, thin thickness, fine mechanical strength and flexibility, and low solubility in electrolytes.[26] The relevant reports on surface chemistry emphasize that the property of SEI critically affects the electrochemical battery performance, and thereby well characterization and control of the films with physical and chemical methods are crucial issues for lithium-ion secondary batteries.[27]

In recent relevant studies of interfaces, the artificial SEIs are also interested, as depicted in Figure 1.7. A development of a water-stable artificial ceramic SEI in the aqueous system is proposed. This solid state lithium-ion conductor is somewhat different from the complicated natural SEI formed by reduction of the electrolyte.[65] Artificial SEIs have advantages in improving the cell performance by reducing irreversible capacity loss due to surface film formation. However the retention of sufficient lithium

ion conductivity in terms of ion conducting film is the most challenging issue in realizing the artificial SEIs.

(a)

A = Li_2O
B = LiF
C = Li_2CO_3
D = Polyolefins
E = Semicarbonates

(b)
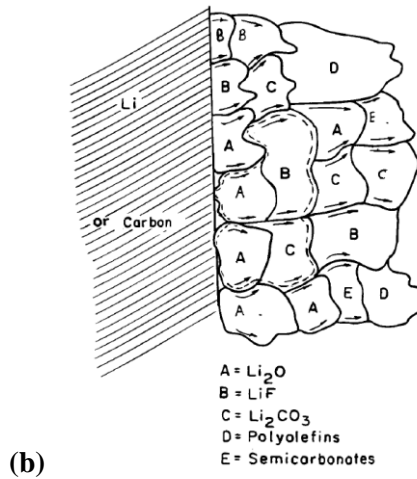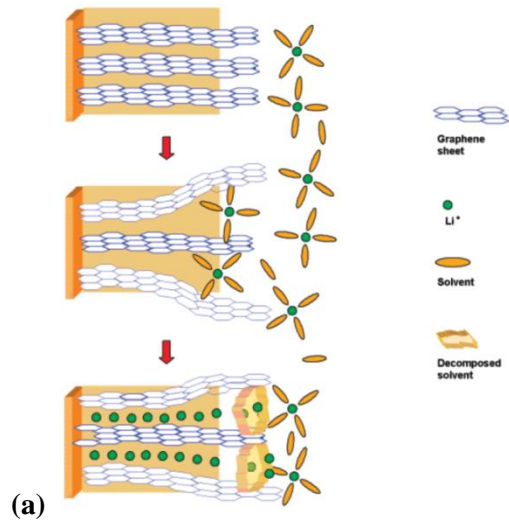
Figure 1.6. (a) Schematic illustration of the SEI formation mechanism *via* the decomposition of non-aqueous electrolyte solvents in battery system.[26] (b) Schematic presentation of a polyhetero microphase SEI on lithium or carbon electrode.[56]
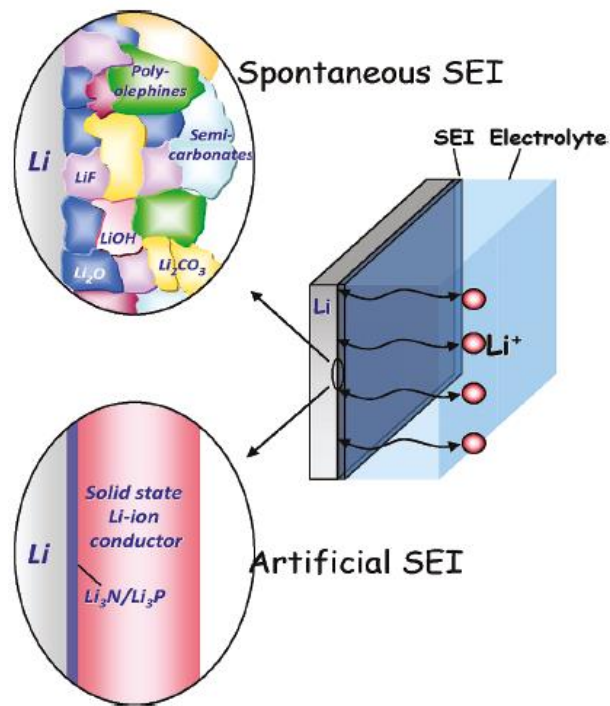
Figure 1.7. Schematic drawing of the lithium metal-electrolyte interface choices. Both of the complicated natural SEI formed by reduction of the electrolyte and an artificial SEI, e.g. lithium-ion conducting ceramic, are shown as examples.[65]

1.4.2. SEI Former Additives

Figure 1.8 demonstrates the schematic diagram of the reduction mechanism of electrolyte solvents and optional additives included in electrolyte at the negative electrode surface. The intercalation of solvated lithium ions into conventional graphite negative electrode occurs at $0 \sim 0.2$ V *vs*. Li/Li$^+$. However an unexpected reaction between lithium ions and electrolytes, generally at the voltage range of $0.4 \sim 0.9$ V *vs*. Li/Li$^+$, arise since the reduction potential of organic solvents, e.g. EC (Figure 1.9(a)), DEC, DMC, are far above than that of lithium ion intercalation into graphite. This step corresponds to SEI formation or generation of the reduced solid products, where the conventional carbonate-based electrolyte decomposition occurs at around 0.5 V *vs*. Li/Li$^+$.

To obtain high quality interface, the change of surface species by using organic additives is regarded as one option. From this vantage point, a use of SEI former additives is widely being studied for prolonged cycle performance accompanied with surface chemistry modification.[28] The presence of SEI former additive molecular moieties in the SEI modifies the entire property and/or chemical structure of the surface films derived by a significant change in the surface reaction. They are reported to be effective in the formation of mechanically and electrochemically stable, highly ion conductive, and thin films. To select and design the appropriate additives for SEI at negative electrode, the reduction tendency of functional materials must be investigated. It is possible to theoretically predict the electrochemical reduction and oxidation tendency through the molecular orbital energy of molecules without experiments. A compound

with a low lowest unoccupied molecular orbital (LUMO) energy value is a good electron acceptor and decomposes more easily at the surface of negative electrode, which forms negative electrode-protecting SEI. This is so called reduction type additive, one of the typical example of SEI former additives.

The reduction type additives undergo preferential electrochemical reduction to electrolyte solvents and form the preliminary film on active material due to their lower LUMO energy level or higher reduction potential.[29] The reduction potential of reduction type additives are slightly higher than that of carbonate solvents, around 0.8 V *vs*. Li/Li$^+$. The preferentially formed SEI *via* reduction type additives stabilizes the negative electrode-electrolyte interface at low potential of 0 V *vs*. Li/Li$^+$. These materials include fluoroethylene carbonate (FEC), vinylene carbonate (VC), vinyl ethylene carbonate (VEC), and vinyl acetate (VA).

FEC depicted in Figure 1.9(b) is a typical reduction type additive, and it is also considered as an alternative co-solvent in electrolyte for a variety of negative electrodes.[30,31,42] The adsorption of FEC-reduced products such as polycarbonates or poly(VC), depicted in Figure 1.9(c), onto active sites of electrode surface assists formation of high quality SEI, and thereby results in the promotion of battery performance. The consecutive chemical reactions to generate polycarbonate are represented in Figure 1.9(d) and (e). The reductive decomposition mechanism of FEC brings out VC and HF molecules generation followed by electrochemically induced polymerization of VC obtained from the precedent reaction owing to a double bond contained in the molecule.[29,42] When the FEC-reduced products are successfully formed at electrode surface, it may lead to a significant impact on the surface film properties.

2 8
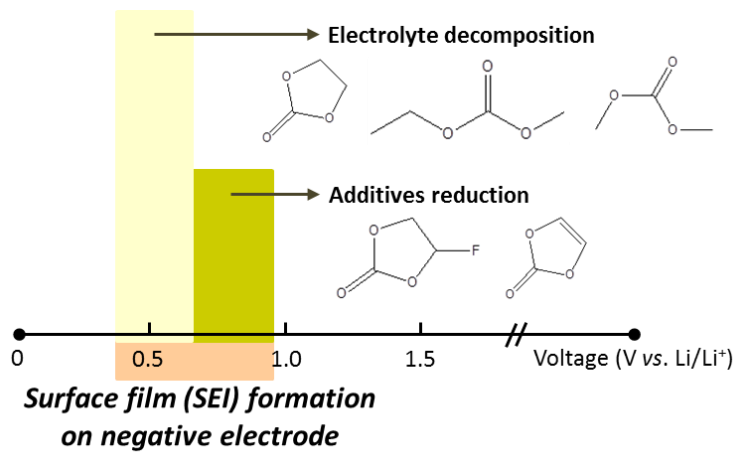
Figure 1.8. Schematic diagram of the reduction mechanism of electrolyte solvents and additives at the negative electrode surface.

(a)   **(b)**   **(c)**   **(d)**   **(e)**
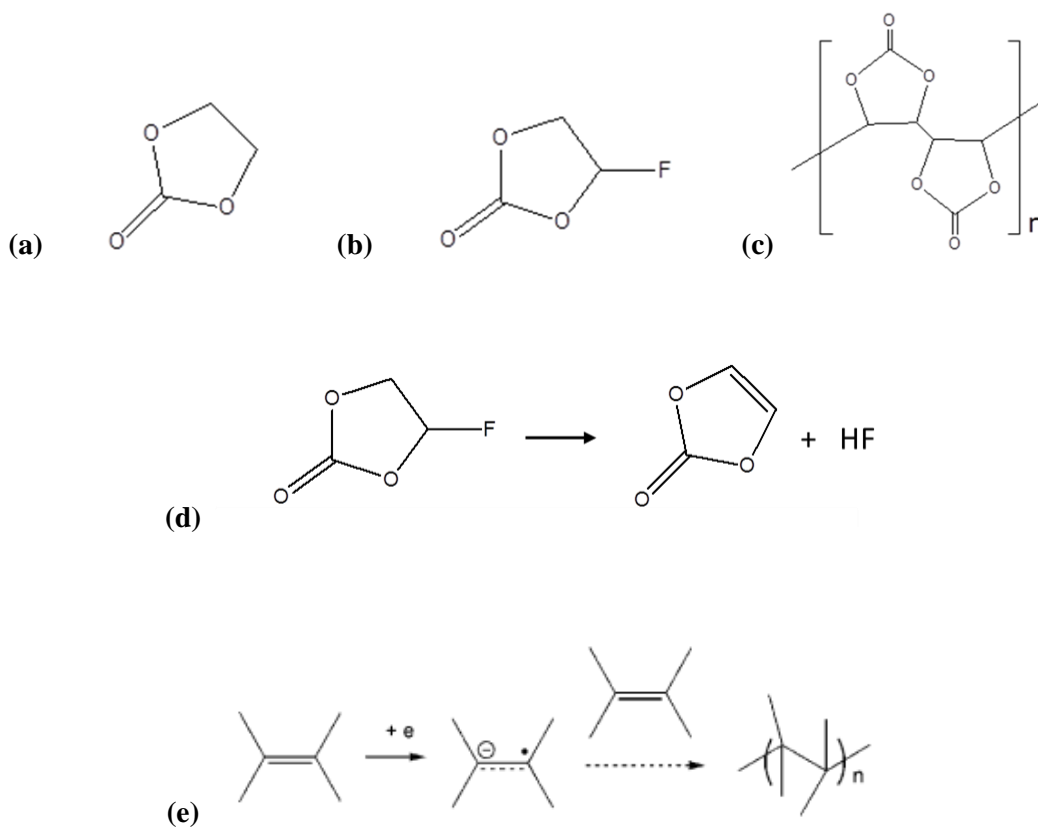
Figure 1.9. Chemical structures of (a) EC, (b) FEC, and (c) poly(VC). (d) Reductive decomposition of FEC followed by (e) electrochemically induced polymerization of VC[29]. The resulting VC and HF from a successful FEC decomposition form insoluble and stable products as the preliminary SEI nuclei.

1.5. Purpose of the Study

In this paper, the positive impact of FEC, reduction type SEI former additive, on the electrochemical battery performance and surface chemistry of nano-sized a-MoO$_2$ negative electrode prepared *via* chemical reduction was investigated. FEC was added in electrolytes as a co-solvent with various contents. The electrolyte system could roughly be classified into FEC-free and FEC-containing system. FEC-containing system is categorized by FEC-based electrolyte that EC is totally replaced with FEC and EC/FEC coexisting electrolytes. The electrochemical battery performance, especially a prolonged cycleability, of a-MoO$_2$ negative electrodes as a function of FEC concentration was investigated.

To find out the underlying relationship between electrochemical behavior of a-MoO$_2$ and FEC involvement, identification of surface chemistry modification depending on the electrolyte system was necessary. The surface characterization was conducted to have an insight into a successive reductive decomposition of FEC on the electrode surface. Electrochemical impedance spectroscopy (EIS), field emission-scanning electron microscope (FE-SEM), attenuated total reflection Fourier transform-infrared spectroscopy (ATR FT-IR), and X-ray photoelectron spectroscopy (XPS) were employed in the characterization.

Based on the findings in electrochemical battery performance and surface characterization, we developed the SEI formation mechanism of EC-derived, FEC-derived, and EC-/FEC-co-derived SEI. A fine understanding of each film properties and their formation mechanism is able to explain the battery performance accompanied with

each surface films. The identification of such mechanisms proposed herein might provide a good idea in understanding the effect of FEC as an effectual alternative co-solvent for modifying the surface chemistry of typical lithium-ion secondary battery negative electrodes. To the best of our knowledge, this is the first report on identifying surface chemistry mechanism of a-MoO$_2$ negative electrode with FEC.

2. Experimental

2.1. Amorphous MoO$_2$ Electrode Preparation

Reduction of aqueous K$_2$MoO$_4$ with proper reducing agent solution at ambient temperature has been investigated to obtain lower valence molybdenum oxides, e.g. MoO$_2$. Alkali metal borohydrides such as NaBH$_4$ and KBH$_4$ can be used as effective reducing agents in aqueous solutions to obtain reduced transition metal oxides. Only MoO$_2$ has been obtained as single-phase product while many compounds are formed during reduction process. The products formed are amorphous in nature, and thereby may become attractive for battery electrodes, catalysis, sensors, optoelectronics, and so forth.[15,63]

2.1.1. Amorphous MoO$_2$ Synthesis

a-MoO$_2$ particles were synthesized *via* generally reported chemical reduction.[15,32] Mo^{6+} aqueous solution (0.25 M K$_2$MoO$_4$ precursor/distilled water) was reduced by separately prepared reducing agent solution (2.5 M KBH$_4$/dilute KOH) to obtain Mo^{4+} or MoO$_2$. Reducing agent solution was slowly injected into precursor solution with hydrochloric acid to form reaction mixture. High pH of reaction mixture caused by KOH solvent is necessary to suppress hydrolysis of borohydride, and prevent rapid loss of hydrogen and of reducing power of borohydride.[32] Meanwhile hydrochloric acid

addition is essential to attain and maintain a target pH value of reaction mixture. A decrease in pH of reaction mixture intensifies condensation of MoO_4^{2-} ions, and the nano-sized particles can be obtained at pH 2. Then the repeated filtering and washing of black colored MoO_2 precipitates obtained from the reaction mixture were followed. The residuals of reducing agent and HCl were washed out to success in desired size and valence of MoO_2 particles. The precipitates were dried at 80℃ for overnight and at 300℃ under vacuum condition for 2 hours for amorphization of them. A schematic diagram of overall procedure of a-MoO_2 synthesis is presented in Figure 2.1(a). X-ray diffraction (XRD) and FE-SEM were employed for characterization of as-synthesized particles.

2.1.2. Electrode Fabrication

The a-MoO_2 composite electrode was fabricated by casting the slurry on 10-µm-thick Cu foil using doctor blade. The slurry consisted of a-MoO_2 active material particle, Super-P conducting agent, and polyvinylidene fluoride (PVdF) binder (7:2:1 in wt%) dispersed in N-methyl pyrrolidone (NMP). Then it underwent drying at 120℃ in vacuum and pressing for the improvement of adhesion strength to the Cu current collector. A schematic diagram of composite electrode and its fabrication process is briefly depicted in Figure 2.1(b). FE-SEM was employed for characterization of as-fabricated electrode. In addition, energy dispersive X-ray spectroscopy (EDS) mapping was conducted to observe the dispersion of active material and its composites on electrode surface.

2.2. Electrochemical Characterization

2.2.1. Galvanostatic Battery Cycling

The electrochemical half-cell tests were conducted with 2032-type coin-cells (Figure 2.2), which was assembled in argon-filled glove box. a-MoO$_2$ electrode (1.1 cm in diameter) and Li foil (Cyprus Co.) were employed as working and counter/reference electrode, respectively, and polypropylene/polyethylene/polypropylene tri-copolymer (Celgard^{TM}) was used as a separator. After assembly, the cells were stored at room temperature for a day to ensure the complete impregnation of the electrodes and separators with electrolyte. 1.3 M LiPF$_6$ was dissolved in the mixture of EC/FEC/diethyl carbonate (DEC) at various volume ratios for electrolyte systems. In this research, FEC was added as a main and/or co-solvent in the electrolytes and varied in its contents. A detail composition of each electrolyte is listed in Table 2.1; EC-based F00 system (1.3 M LiPF$_6$/EC:DEC = 30:70 vol%), FEC-based F30 system (1.3 M LiPF$_6$/FEC:DEC = 30:70 vol%), and EC/FEC coexisting F20, F10 system (1.3 M LiPF$_6$/EC:FEC:DEC = 10:20:70 vol%, 1.3 M LiPF$_6$/EC:FEC:DEC = 20:10:70 vol%). The galvanostatic charge/discharge cycling was conducted at constant current density of 100 mA/g and cut-off voltage of 3.00 V ~ 0.01 V (vs. Li/Li$^+$) using an automatic battery cycler (WBCS3000, WonA Tech. Co.) at room temperature, 25℃. In this paper, lithiation and delithiation refer to charge and discharge process, respectively.

2.2.2. Electrochemical Impedance of Charge Transfer

EIS was applied to investigate the interfacial lithium ion charge transfer resistance. The main problem associated with EIS measurements is the ambiguous interpretation of the spectral features.[68] Nevertheless, EIS can be an efficient technique for comparing the general behavior of electrode-electrolyte interfaces. Alternating current (AC) impedance of the coin-cells was potentiostatically measured (Parstat 2273) in the frequency range of 0.1 Hz ~ 100 kHz and AC voltage amplitude of 5 mV. Impedance spectra were measured at the state of equilibrium potential, 2.0 V, after delithiation to guarantee equivalent state of discharge.[45] The interpretation was possible after spectra fitting by Z-view program.

2.3. Surface Analysis

After electrochemical analyses, a-MoO$_2$ electrodes were removed from the coin-cells and rinsed with dimethyl carbonate to eliminate residual electrolyte. The microscopic and spectroscopic investigations were employed for surface chemistry characterization of the cycled electrodes after certain cycles. FE-SEM was used for microscopic observation of SEI morphology and electrode structure. Qualitative analysis of chemical composition of surface films was accomplished by ATR FT-IR (Nicolet 6700) and XPS (Sigma Probe). Additionally, the thickness of surface films derived by different electrolyte components could be indirectly estimated with XPS spectra. All of the surface characterizations were carried out in the state of delithiated a-MoO$_2$ electrodes in *ex-situ* mode.

(a)

Precursor solution:
0.25 M K_2MoO_4/distilled water

Reducing agent solution:
2.5 M KBH_4/dilute KOH

* pH 11

pH control of reaction mixture:
- reducing agent injection into precursor solution
- HCl addition

* Attain and maintain the pH 1 ~ 4

Precipitate filtering/washing

- Drying at 80°C for overnight
- Drying at 300°C for 2 hours in vacuum

Amorphous MoO_2 (a-MoO_2)

* Synthesized at pH 2 of reaction mixture

Slurry composition:
Active material: a-MoO_2
Conducting agent: Super-P
Binder: polyvinylidene fluoride (PVdF)
Solvent: N-methyl pyrrolidone (NMP)
a-MoO_2:Super-P:PVdF=7:2:1 wt%

Doctor blading on Cu foil
Drying at 120°C in vacuum
Roll-to-roll pressing
Working electrode of 1.1 cm in diameter

Liquid electrolyte

Cu current collector

● Active material ● Conducting agent ● Binder

◯ SEI layer → Li ion pathway

(b)

Figure 2.1. (a) Schematic diagram of amorphous MoO_2 synthesis procedure. (b) Schematic diagram of composite electrode fabrication process and its configuration.
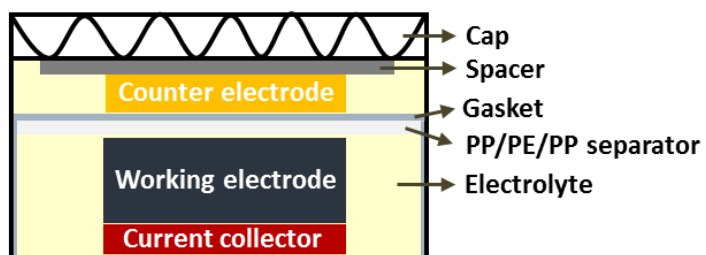
* Counter/reference electrode: Li foil (Cyprus Co.)

* Separator: PP=polypropylene, PE=polyethylene (Celgard™)

* Current collector: Cu foil (10 μm)

Figure 2.2. Schematic diagram of 2032-type coin-cell.

Table 2.1. Electrolyte Conditions with Various FEC Contents. F00 Stands for FEC-free System and The Rest of Electrolytes Are FEC-containing System with A Gradual Change in FEC Concentration

Electrolyte abbreviation	Li salt	Organic solvents (in vol%)		
		EC	FEC	DEC
F00	1.3 M LiPF$_6$	30	-	70
F30		-	30	70
F20		10	20	70
F10		20	10	70

3. Results and Discussion

3.1. Electrode Characterization

a-MoO$_2$ particles were obtained from the prepared reaction mixture of Mo^{6+} aqueous solution and reducing agent solution. The crystallinity and oxidation state of the active material was analyzed by XRD. The oxidation state of the synthesized a-MoO$_2$ can be estimated by crystallization of a-MoO$_2$ (c-MoO$_2$). c-MoO$_2$ was obtained by annealing a-MoO$_2$ at 600℃ in argon atmosphere for 4 hours. Figure 3.1(a) shows each sample of a-MoO$_2$ and c-MoO$_2$.

XRD peak for as-synthesized a-MoO$_2$ particle (Figure 3.1(b), blue line) demonstrates a broad pattern, indicating that the synthesized MoO$_2$ particles were amorphous. XRD pattern of c-MoO$_2$ is shown as a red line in Figure 3.1(b). The patterns nearly correspond to those of the monoclinic MoO$_2$ phase (MoO$_2$ JCPDS No. 32-0671). However a marginal amount of the other reduced chemical of molybdate solution, Mo$_4$O$_{11}$, is detected along with MoO$_2$ phase. It is contributed to the partial insufficient reduction of Mo^{6+} during the synthesis and/or a slight surface oxidation of metastable MoO$_2$ in air.[33,71] Figure 3.1(c) demonstrates the FE-SEM image of the nano-sized material in size of approximately 100 nm.

The composite electrode fabricated with a-MoO$_2$ nanoparticle exhibited roughly 40 μm in thickness (Figure 3.2(a)). The electrode showed a good bonding between active material composite and current collector, and continuous contact of the composites. A

fine surface morphology without much of agglomeration among the particles was confirmed from the surface image of the as-fabricated electrode (Figure 3.2(b)). The uniform dispersion of active material and other components is an important factor for an even current flow inside electrodes and to prevent local over(dis)charge. To support a good dispersion of the slurry, EDS mapping was additionally conducted. The homogeneous distribution of a-MoO$_2$ and other components of slurry were observed as shown in Figure 3.2(c). The elements of interest were Mo, O, C, and F. Mo and O, C, and F were originated from active material, conducting agent, and PVdF binder, respectively.

(a)

(b)

(c)
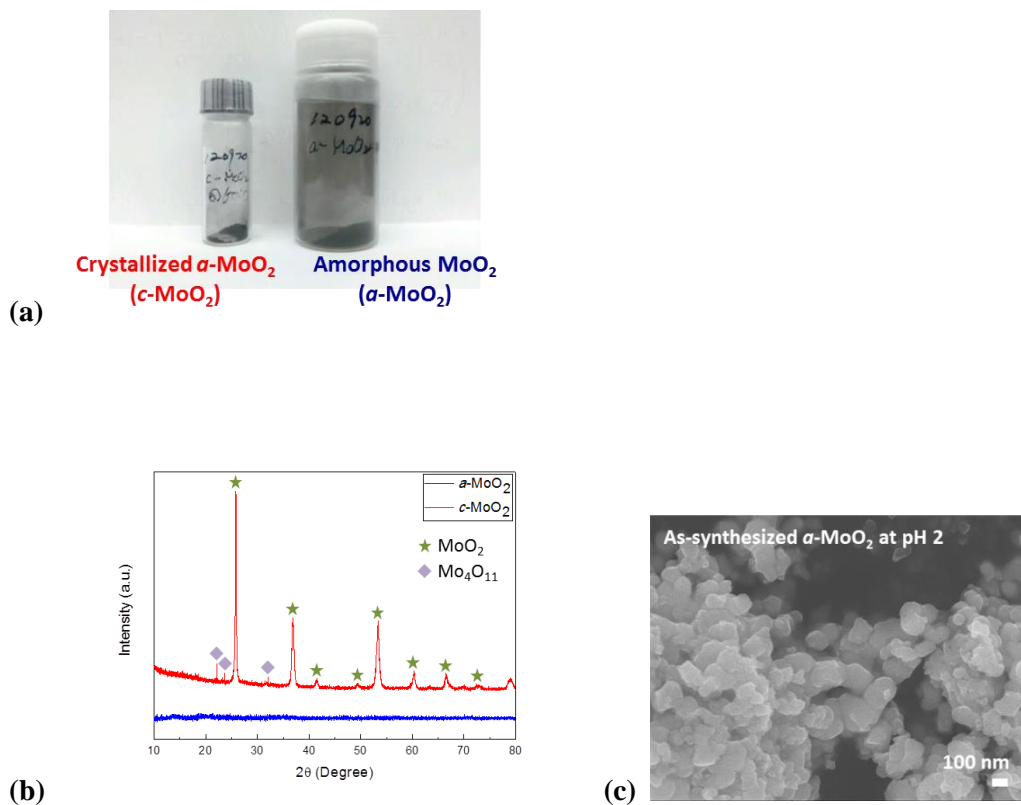
Figure 3.1. (a) Sample images of c-MoO_2 (left) and a-MoO_2 (right) particles. (b) XRD patterns of a-MoO_2 (blue line) and c-MoO_2 (red line) particle. (c) Microscopic investigation of as-synthesized a-MoO_2 particles, which exhibited the size of approximately 100 nm.
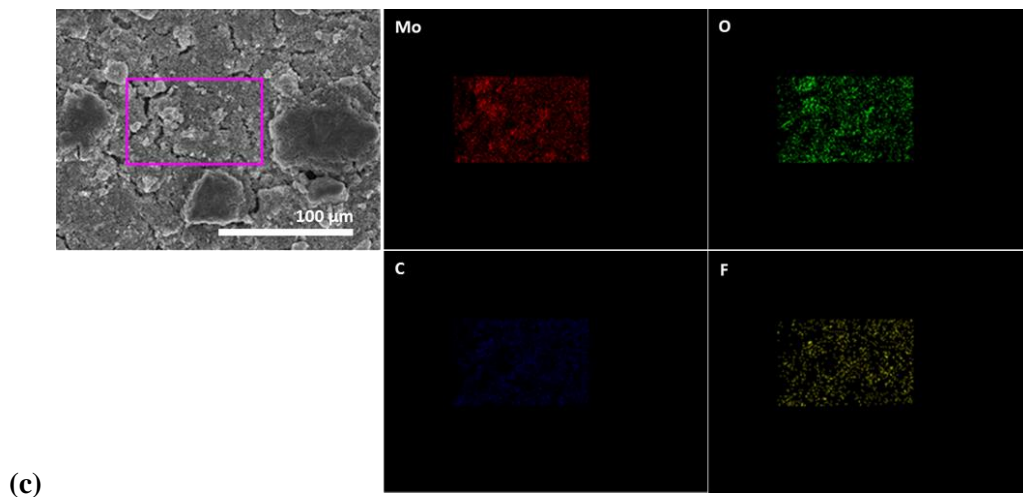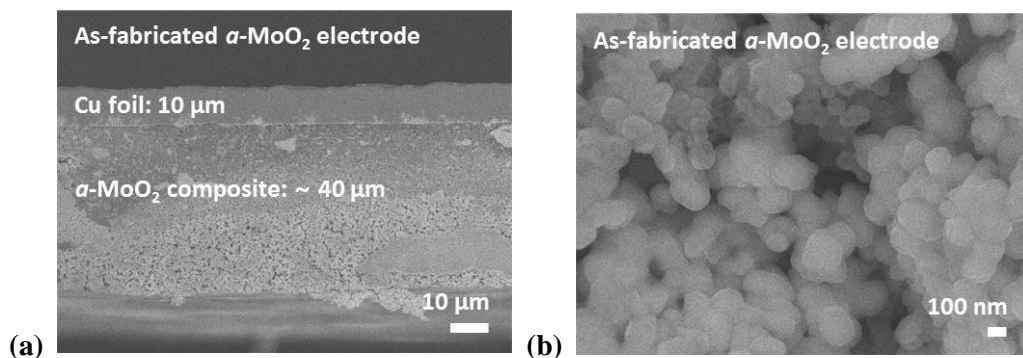
Figure 3.2. FE-SEM images of (a) cross-sectional and (b) surface view of the as-fabricated a-MoO$_2$ composite electrode. The cross-section image is obtained after cross-sectional polishing in argon. (c) EDS mapping of the as-fabricated electrode.

3.2. Electrochemical Battery Performance

3.2.1. Electrochemical Behavior

From the reversible reaction of a-MoO_2 nanoparticle with lithium ions, the nano-sized molybdenum metal particles that are dispersed in the Li_2O matrix are formed by lithiation but restored to the original oxides by delithiation.[23,35-37] Figure 3.3(a) demonstrates voltage profiles obtained from each electrolyte system. The sloping voltage profiles indicate lithium ion storage sites are continuous and electrochemically nonequivalent in active material, which has amorphous disordered atomic-scale structure.[38] From the differential capacity plot (Figure 3.3(b)), the chemistry change responsible for lithium ion storage behavior and phase transformation of active material during cycling could be informed. The conversion reaction plateau was observed from lithiation peak at around 0.4 V, which was attributed to the reaction of a-MoO_2 ((1)). The conversion reaction for the second and consecutive lithiation of typical transition metal oxides differ from that of the first lithiation due to the formation of intermediates.[23] In the same manner, the plateau of its structurally transformed intermediate oxide, $MoO_{2+\delta}$, is a bit shifted ((2)). The two amorphous delithiaion peaks ((3), (4)) appeared throughout electrochemical cycling. It is ascribed to the maintenance of amorphous structure after repeated full charge and discharge without transition to crystalline phases.[39,40]

Figure 3.4 shows the specific capacity, coulombic efficiency, and discharge capacity retention of a-MoO_2 negative electrode cycled in four different electrolytes. Superior

reversible capacities in the presence of FEC can be explained by reduction in lithium ion consumption during the first cycle for SEI formation and/or lithium ion trapping inside the a-MoO$_2$ matrix.[41] A close investigation of initial specific capacity in each electrolyte informed that the first delithiation capacity was slightly increased as a function of FEC content. Since FEC-containing system reduces irreversible capacity loss for surface film formation, it could enhance the reversible reaction of lithium ions with active material. It is also reflected in the coulombic efficiency. Coulombic efficiency is closely related to the interfacial issues since it originates from lithium ion migration across the surface films along with lithium solid diffusion in active material. Coulombic efficiency of cells cycled in FEC-containing system was close to 99%, which was higher than that of FEC-free system. It implies the surface films formed in the presence of FEC allowed easy and fast lithium ion migration. Finally a-MoO$_2$ cycled in FEC-containing system resulted in promotion of discharge capacity retention as a function of FEC content (Figure 3.4(c)). It is clear that the more FEC involved in the electrolyte, the better the cycling performance. Especially when EC was totally replaced by FEC, the capacity retention was 82.75% after 50 cycles, which was about 7% higher than that cycled in F00 electrolyte. A promotion in cycleability and other electrochemical behavior with FEC addition must originate from the surface reaction modification.

A superior film must possess appropriate ion conductivity, mechanical and electrochemical stability, and so forth throughout the cycling, which minimizes the battery degradation. To have an insight into the underlying relationship between the battery performance and superior SEI formation, the surface characterization was conducted.
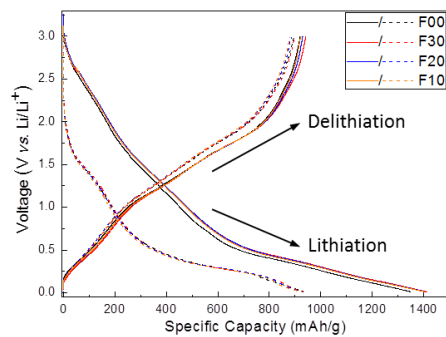
(a)
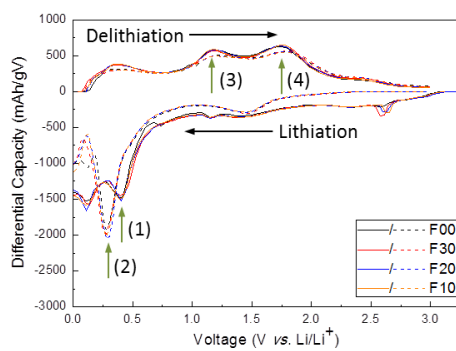
(b)

Figure 3.3. (a) Voltage profiles and (b) differential capacity plots of the cells cycled in FEC-free and FEC-containing electrolytes. The solid and dashed lines indicate the first and third de-/lithiation curves, respectively.

(a)

(b)

@ 50th cycle	Capacity retention (%)
F00	75.63
F30	82.75
F20	80.59
F10	79.97
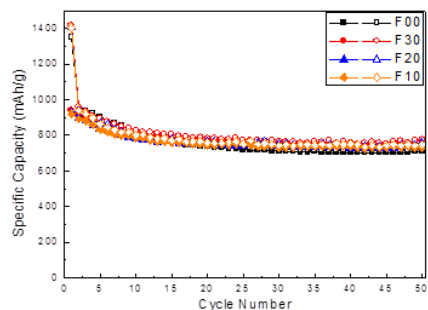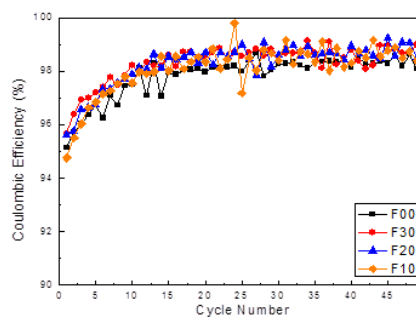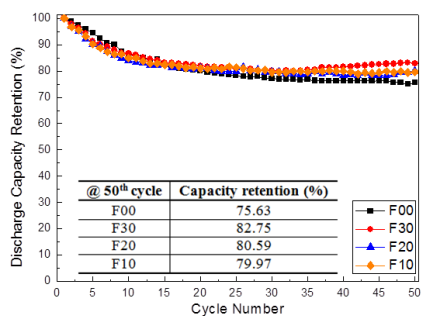
(c)

Figure 3.4. (a) Specific capacity of a-MoO$_2$ negative electrode cycled in different electrolytes. The closed and open symbols refer to delithiation and lithiation capacity, respectively. (b) Coulombic efficiency and (c) discharge capacity retention results for 50 cycles. A table of capacity retention values is supported in the inset of (c).

3.2.2. Electrochemical Impedance Spectroscopy

The kinetics of lithium ion migration across interfaces in battery system can be measured with EIS technique. Nyquist plot consists of two semicircles in high frequency region that attributes to charge transfer process and a sloped line in low frequency region related to mass transfer process of lithium ions. Semicircles in high frequency region can be deconvoluted into two semicircles by Z-view fitting program based on corresponding equivalent circuit (Figure 3.5(a)). The first semicircle represents the charge transfer between electrolyte-SEI and across the SEI, R_{SEI}, and the second semicircle signifies the charge transfer between SEI-active material, R_{CT}. R_{sol} stands for ohmic resistance of electrolyte, C_{SEI} and C_{dl} for capacitance of SEI and double layer capacitance on a-MoO$_2$, respectively, and Z_w refers to Warburg impedance describing solid state diffusion of lithium ions.[31,42-45]

Investigation of impedance spectra after 50 galvanostatic cycles in F00, F30, and F20 electrolytes was performed in order to address the different charge transfer phenomena related to the surface films formed in FEC-free and FEC-containing systems. Further analyses for F10 electrolyte are omitted since F20 electrolyte can represent the system of which EC and FEC coexist in electrolyte. Impedance spectra were measured at the state of equilibrium potential, 2.0 V, after delithiation to guarantee equivalent state of discharge.[45] Figure 3.5(b) and Table 3.1 demonstrate the impedance spectra and resistance values, respectively. FEC-derived SEI formed from F30 electrolyte exhibited the lowest R_{SEI} and R_{CT}, and *vice versa* for EC-derived SEI from F00 electrolyte. EC-

/FEC-co-derived SEI formed from F20 electrolyte showed higher R_{SEI} and R_{CT} than those of FEC-derived SEI, but lower than those of EC-derived SEI. It was indicative that FEC addition possessed a critical role in lowering the charge transfer resistance of the films, hence increased the ion conductivity of FEC-derived and EC-/FEC-co-derived SEIs. R_{sol} in all the cases was negligible compared to other resistance parameters in studying charge transfer phenomena of surface films, and thereby excluded in calculation of the total charge transfer resistance.

Additionally, we measured the impedance of each system for several selected cycles to observe their variation upon cycling. The impedance variation is considered to be determined by the lithium ion migration distance and electrical properties of surface species. Therefore it reflects the surface film thickening as well as lithium ion conductivity of the films. Figure 3.6(a) summarizes the variation of R_{SEI} alone, which indicates resistance associated with lithium ion migration at the interface of electrolyte-SEI and across the SEI. Figure 3.6(b) demonstrates the variation of the sum of R_{SEI} and R_{CT}, which refers to the total resistance for interfacial faradaic charge transfer reaction of lithium ions. In both results, charge transfer resistance of the films formed in FEC-containing system kept at lower level throughout the whole cycling. It was indicative of the ease of interfacial charge transfer between a-MoO_2 negative electrode and FEC-derived and/or EC-/FEC-co-derived SEI. Hence we could conclude that hindered film thickening and higher lithium ion conductivity in electrolyte-SEI-active material system could be achieved with FEC due to the positive impact of FEC-reduced products.
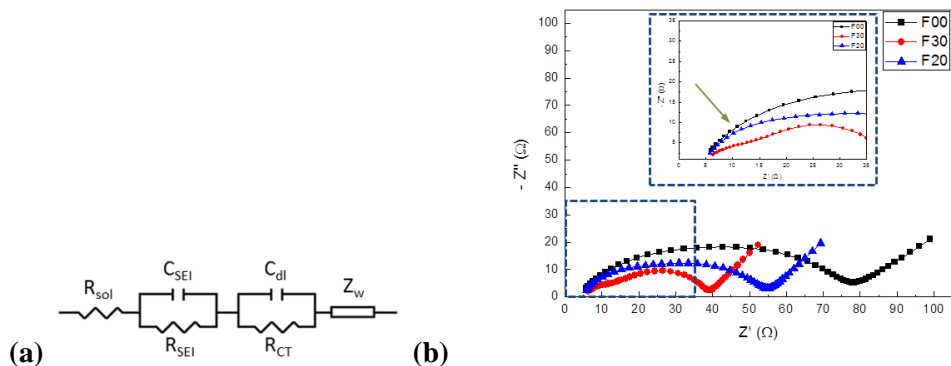
Figure 3.5. (a) An ordinary equivalent circuit used in impedance data fitting and (b) Nyquist plots obtained after 50 cycles in three different electrolytes. The green arrow in the inset of (b) indicates the first semicircle, R_{SEI}.

Table 3.1. A Table of Resistance Values: R_{sol}, R_{SEI}, and R_{CT}. The Total Resistance for Interfacial Faradaic Charge Transfer Reaction of Lithium Ions Is Calculated by Adding Up R_{SEI} and R_{CT}, which Are The Main Parameters that Reflect The Charge Transfer Phenomena of Surface Films

R (Ω)	R_{sol}	R_{SEI}	R_{CT}	$R_{SEI} + R_{CT}$
F00	4.0	31.8	40.0	71.8
F30	4.6	11.5	22.5	33.9
F20	4.6	16.2	33.7	49.9
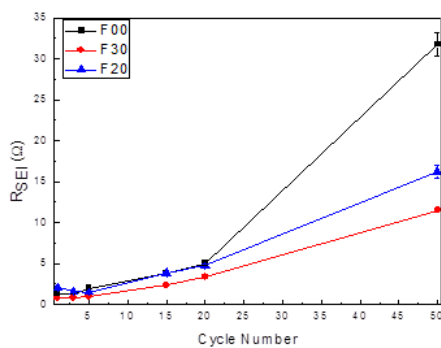
(a)
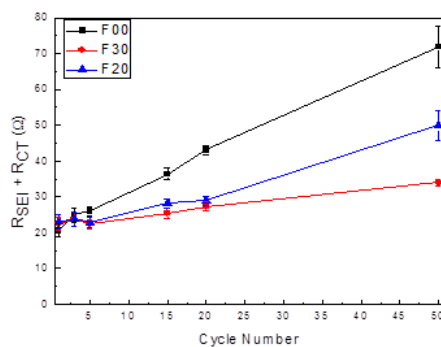
(b)

Figure 3.6. The variation of (a) R_{SEI} and (b) $R_{SEI} + R_{CT}$ for each surface film upon cycling. Previous capacity retention and total interfacial faradaic charge transfer resistance upon cycling exhibited a clear gap for FEC-free and FEC-containing system beginning from the 15th cycle.

5 1

3.3. Surface Characterization

The modification of surface chemistry at the electrode surface using SEI former additives depends on the electrode nature.[46] Thus it is essential to understand the surface chemistry of a-MoO$_2$ negative electrode with and without FEC in electrolytes studied herein. To have an insight into the relationship between the improvement in battery performance discussed so far and features of surface films influenced by FEC, the EC-derived, FEC-derived, and the EC-/FEC-co-derived SEI were characterized by using *ex-situ* FE-SEM, FT-IR, and XPS.

3.3.1. Field Emission-Scanning Electron Microscope

FE-SEM images of a-MoO$_2$ electrodes after 50 cycles in FEC-free and FEC-containing electrolytes are presented in Figure 3.7. The foreign materials were deposited on the electrode surfaces compared to as-fabricated electrode and/or as-synthesized particles, which must be the surface films.[47,70] The SEIs derived from FEC-free and FEC-containing system effectively covered the active materials with smooth and uniform morphology. Fine film morphology guarantees the even flow of electrons and ions through the film, and the mechanical stability of SEI itself upon repetitive cycling as well.

Additionally the electrodes observed herein retained their structure upon cycling without severe damages such as pulverization of particles, mechanical and/or electronic contact loss of active material and current collector. Then it can be concluded that the

battery performance degradation mainly resulted from the surface film properties rather than the electrode degradation. As demonstrated further in this paper, it appears that the presence of FEC induces the obvious and pronounced effect on the surface chemistry of a-MoO$_2$ negative electrodes.
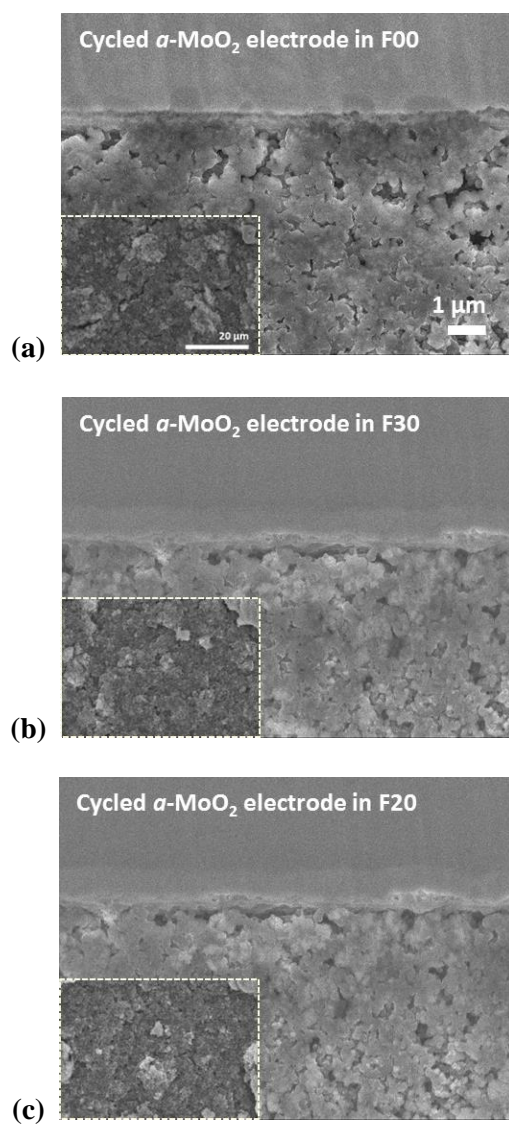
Figure 3.7. The cross-sectional and surface (inset) images of delithiated a-MoO$_2$ electrodes cycled in (a) F00, (b) F30, and (c) F20 electrolytes, respectively, after 50 cycles.

3.3.2. Attenuated Total Reflection Fourier Transform-Infrared Spectroscopy

   Apparent difference in the surface species formed in different electrolytes was identified from ATR FT-IR spectra as shown in Figure 3.8. For state-of-the-art electrolytes, the reduction of cyclic carbonates such as EC and FEC should provide the major species to build up surface films while the participation of linear carbonates such as DEC should be relatively inconsequential.[48] Therefore the reduced products must be determined by the reduction reactivity of the cyclic carbonate solvents which is in order of FEC>EC>DEC herein.[42]

   EC-derived SEI (Figure 3.8(a)) was composed of lithium carbonate organics and inorganics as a result of EC reduction. It was dominant in oxygen-containing products such as lithium alkyl carbonate (ROCO$_2$Li), lithium carbonate (Li$_2$CO$_3$), and lithium ethylene dicarbonate ((CH$_2$OCO$_2$Li)$_2$). On the contrast, spectra related to FEC-derived SEI (Figure 3.8(b)) were completely different from those related to EC-derived SEI. The main spectral features were that it was rich in polycarbonates (peaks around 1800 cm^{-1}) and alkoxy species (1200 ~ 1000 cm^{-1}) which were absent in EC-derived SEI. FEC in the electrolyte undergoes reductive decomposition and elimination of HF on the active surface of electrode, which forms VC that readily proceed to electrochemically induced polymerization *via* its double bond to form polycarbonate and LiF surface species.[29,42] The polycarbonates derived by such a chemical reaction provide superior flexibility of the film upon volume change of underlying *a*-MoO$_2$, which originates from the intrinsic property of polymeric species.[28] Flexible surface films derived by FEC ensure less

mechanical and electrochemical damage on the films, and thereby decrease in irreversible capacity loss for the additional formation of the film upon repetitive cycling. In the case of EC-/FEC-co-derived SEI (Figure 3.8(c)), the spectra were similar to those that belong to EC-derived SEI but they contained FEC-reduced products as well. The pronounced peaks of both lithium carbonate compounds and polycarbonates imply that although the reduction reactivity of FEC is stronger than that of EC, EC reduction competitively occurred in the SEI formation. Hence EC-/FEC-co-derived SEI may retain the benefits of FEC-reduced products as well as drawbacks of EC-reduced products in the process of surface film formation.

These reduced solid products in each system significantly affect the film properties that are responsible for corresponding prolonged capacity retention. EC-derived SEI that is rich in EC-reduced lithium carbonates allows easier electrolyte penetration into the active material through the microvoids inside its chemical structure. Moreover the film must be comparatively inflexible which cannot endure a massive volume change of underlying active material, and results in additional formation of surface film or reduced products to recover exposed active surface to electrolyte. Such phenomena lead to film thickening and drastic irreversible capacity loss of EC-based cell. However when FEC is involved, FEC-derived and EC-/FEC-co-derived SEI which are abundant in FEC-reduced polycarbonates result in compact or dense chemical structure that can prohibit further contact of electrolyte and active material. And flexible polycarbonate-based films can sufficiently endure the electrode deformation that guarantees mechanical stability of SEI itself. These antithetic factors can greatly affect high quality interfaces, and thereby can achieve notable improvement in the battery performance.
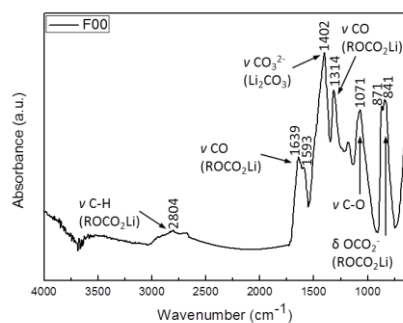
(a)
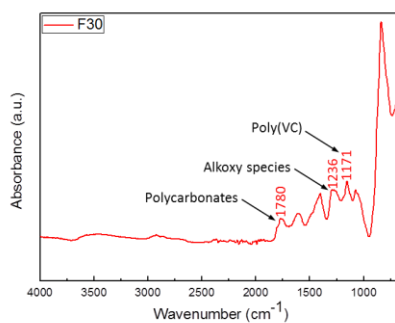
(b)
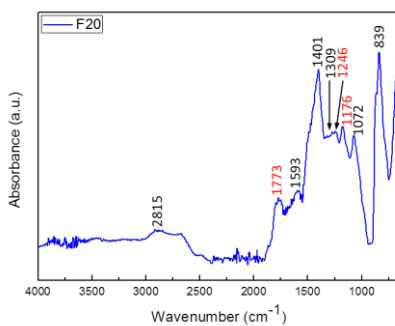
(c)

Figure 3.8. ATR FT-IR spectra of surface films formed on a-MoO$_2$ electrodes in (a) F00, (b) F30, and (c) F20 electrolytes after 50 cycles. The numbers in the figures represent the wavenumber of corresponding peaks. In the case of (c), black letters and red letters refer to EC-reduced products (excerpted from (a)) and FEC-reduced products (excerpted from (b)), respectively.

3.3.3. X-ray Photoelectron Spectroscopy

Further qualitative investigation of the surface species derived by FEC-free and FEC-containing system was conducted with XPS. The high-resolution XPS spectra exhibited a significant difference in the chemical structure of the SEIs that can reflect the chemical composition, thickness, and ion conductivity of the films. Mo 3d, F 1s, O 1s, C 1s, Li 1s, and P 2p spectra were employed to obtain chemical information about the active material and the surface films. Following Figure 3.9 represents the survey spectra of cycled electrodes in different electrolyte systems.

The XPS spectra of as-fabricated a-MoO$_2$ electrode were employed to identify electronic state of the a-MoO$_2$ active material. The survey spectra, Mo 3d and O 1s high-resolution spectra of the electrode before conducting galvanostatic battery cycling are given in Figure 3.10. High-resolution XPS spectra of Mo 3d (Figure 3.10(b)) exhibited two dominant peaks corresponding to Mo^{4+} 3d$_{3/2}$ (233.1 eV) indicating Mo^{4+} oxidation state of MoO$_2$ and Mo^{6+} 3d$_{3/2}$ (236.2 eV). The existence of Mo^{6+} is contributed to the partial insufficient chemical reduction of aqueous Mo^{6+} solution during the synthesis and the possible surface oxidation of the metastable particle in air.[33,49,71] It is consistent with previous XRD pattern of as-synthesized a-MoO$_2$ particles after crystallization. The naturally formed Mo^{6+} does not serve as an active electrode material. Then it is suitable to interpret the existence of Mo^{6+} as it was disproportionated into Mo^{4+} active material[69] rather than Mo^{4+} and Mo^{6+} were separated or segregated within the active matrix.

The asymmetric O 1s XPS spectra (Figure 3.10(c)) were deconvoluted into three peaks,

O_a (530.9 eV), O_b (531.4 eV), and O_c (532.5 eV). The O_a peak on the low binding energy of O 1s spectra is attributable to the Mo-O bonds and the O_c peak on the higher binding energy contributes to residual oxygen-containing group on the surface of the MoO_2 particle.[57] The O_b peak at the medium binding energy is associated with O^{2-} ions that are in oxygen-deficient regions within MoO_2 matrix.[58] It indicates the amorphous structure of the active material provides a number of structural defects such as oxygen or molybdenum vacancies, which possesses the free volumes that accommodate lithium ions.

High-resolution XPS spectra of Mo 3d (Figure 3.11(a)) for cycled electrodes were deconvoluted into four dominant peaks according to the oxidation and surface electronic state of molybdenum; the binding energies of the Mo^{4+} $3d_{3/2}$ and Mo^{4+} $3d_{5/2}$ peaks exist at 232.7 eV and 229.3 eV, respectively, along with the Mo^{6+} $3d_{3/2}$ and Mo^{6+} $3d_{5/2}$ at 235.8 eV and 231.4 eV, respectively. A clear result of the relative surface film thickness could be obtained by comparing the peak intensity of interfacial Mo^{4+} for the electrodes cycled in each electrolyte system. The amount of active material at the electrode surface can reflect the thickness of the surface film.[42,50] The higher intensity of active material implies the thinner SEI is formed at active material surface, and the opposite is exactly the same. Figure 3.11(b) summarized the peak area of total interfacial Mo^{4+} in each electrolyte system on the basis of quantitative analysis of the XPS spectra. FEC-free system exhibited the lowest Mo^{4+} peak intensity indicating the thickest SEI formed on electrode surface. On the other hand, FEC-containing systems showed relatively higher Mo^{4+} content in the surface species as a function of FEC concentration. It implies that the presence of FEC resulted in the formation of thin surface films.

F 1s high-resolution XPS spectra (Figure 3.12) exhibited pronounced peaks of fluorine salts in the surface species. They were C-F bonding obtained from PVdF binder, Li_xPOF_y and Li_xPF_y species (687.7 eV), and LiF material (685.2 eV).[44,51,52] The content of LiF increased as a function of FEC concentration on the basis of quantitative analysis of the XPS spectra. A high LiF level is attributed to the HF obtained from successive reductive decomposition of FEC which transforms lithium carbonates that already exist in the film to LiF.[52-54] LiF-rich surface films can significantly enhance the impermeability to electrolyte due to its insolubility, and thereby guarantees the electrochemical stability of the films. Moreover based on the fact that LiF inorganic is conductive component compared to organics in surface species, it is indicative that abundant LiF can reduce the charge transfer resistance of lithium ions that leads to high lithium ion conductivity across the film. Interfacial LiF in the surface film is a major compound that is able to explain the low electrolyte permeability and high ion conductivity of the FEC-derived and EC-/FEC-co-derived SEI,[44,50-52] which is responsible for increased reversible capacity for prolonged cycling.

The reduction of alkyl carbonate solvents and/or organic additives, which is the primary process for the surface film formation, results in organic and inorganic lithium salts represented by high amounts of oxygen and carbon. Figure 3.13 demonstrates that the O 1s high-resolution XPS spectra possessed the different amounts and types of oxygen-containing materials depending on different electrolyte systems. The reduced products of electrolyte solvents are fitted based on the relevant reports.[42,44,55] The EC-derived SEI mainly contained a peak of $-CO_3-$ (531.8 eV) that contributes to Li_2CO_3 and $ROCO_2Li$, which are typical EC-reduced products, whereas C=O (532.5 eV) and -O-

(533.5 eV) that are related to polycarbonates were negligibly discovered. And it was notable that Li_2O and/or O_2 (528.8 eV) peak was observed which was absent in FEC-derived and EC-/FEC-co-derived SEI. The existence of Li_2O and/or O_2 seems originated from surface oxidation caused by imperfect passivation of EC-derived SEI. On the other hand, FEC-reduced polymeric species were dominantly built up in FEC-derived SEI. The FEC-reduced products were abundant in C=O and -O- bonding. C=O is a chemical bonding that can be observed from chemical structure of polycarbonates and -O-, bridge oxygen or ether, indicates phosphates or oxygen-containing polymeric species. Moreover alkoxide (ROLi, 530.8 eV) is another evident FEC-reduced product that was detected with the presence of FEC, consistent with what was observed in the previous FT-IR spectra. EC-/FEC-co-derived SEI showed similar spectra to those belong to FEC-derived SEI. Although FEC is preferentially reduced and alleviates the accumulation of EC-reduced products, both FEC- and EC-reduced solid products participate in the film formation competitively at the first and the following charge processes.[42] Therefore the main components of EC-/FEC-co-derived SEI were similar to those of FEC-derived SEI, but lower in FEC-reduced products content and higher in EC-reduced products content.

High-resolution C 1s XPS spectra are in line with the O 1s spectra, implying the surface film formed in electrolyte without FEC is rich in lithium carbonates, whereas those formed in electrolytes in presence of FEC are relatively rich in polycarbonates and alkoxide. Figure 3.14 shows all the organic species containing carbon atom. C (284.2 eV) is originated from conducting agent and other carbon-containing materials, and hydrocarbon (285.0 eV) refers to both polycarbonates and lithium carbonates. CH_2CH_2O (285.7 eV), CH_2O (286.6 eV), O-C-O, C=O (287.6 eV), and O-C=O (289.8 eV) are

related to the carbon bonding in polycarbonates while -CO_3- (290.5 eV) is related to the carbon bonding in Li_2CO_3 and $ROCO_2Li$. EC-derived SEI was dominant in Li_2CO_3 and $ROCO_2Li$ but negligible in polycarbonates group, whereas FEC-derived and EC-/FEC-co-derived SEI were abundant in polycarbonates but lack in lithium carbonates. In a word, FEC-reduced products support superior quality of SEI due to their material properties, and they constitute the surface films as a function of FEC content. Hence such a surface chemistry modification is the main factor that affects the battery performance of each system as discussed so far.

Li 1s high-resolution XPS spectra (Figure 3.15) exhibited a broad peak centered at around 55 eV, which are attributable to LiF (55.6 eV), lithium (alkyl) carbonate (54.8 eV), and other salts containing lithium atom. The reduction in total peak intensity of FEC-containing system indicates that the lithium concentration in the film decreases with FEC addition. In other words, lithium consumption is suppressed during the first and the following cycles for SEI formation in FEC-containing electrolytes,[44] which is responsible for reduced irreversible capacity loss for side reaction of lithium ions or enhanced reversible reaction of them with active material. Additionally the content of LiF and lithium carbonate in three different surface films could be reconfirmed from the corresponding peaks.

High-resolution XPS spectra of P 2p (Figure 3.16) reflected the formation of surface species related to the reduction of the PF_6^- anion which is contained in $LiPF_6$ salt. The possible anion reduction products include Li_xPF_y and Li_xPOF_y species,[42] which were investigated in F 1s spectra as well. Additionally, an increase in F and HF generated from FEC reductive decomposition might have resulted in higher content of anion reduction

products since they are the reacted salts obtained from lithium salt and/or electrolyte.

From the combined FT-IR and XPS results, we could conclude that EC-derived, FEC-derived, and EC-/FEC-co-derived SEI have notable differences in their components and thickness. It is directly related to distinguished property and chemical structure of each surface film. Such differences in electrochemical property of surface films significantly affect the prolonged electrochemical battery performance accompanied with SEI stability issue.

(a)

(b)

(c)
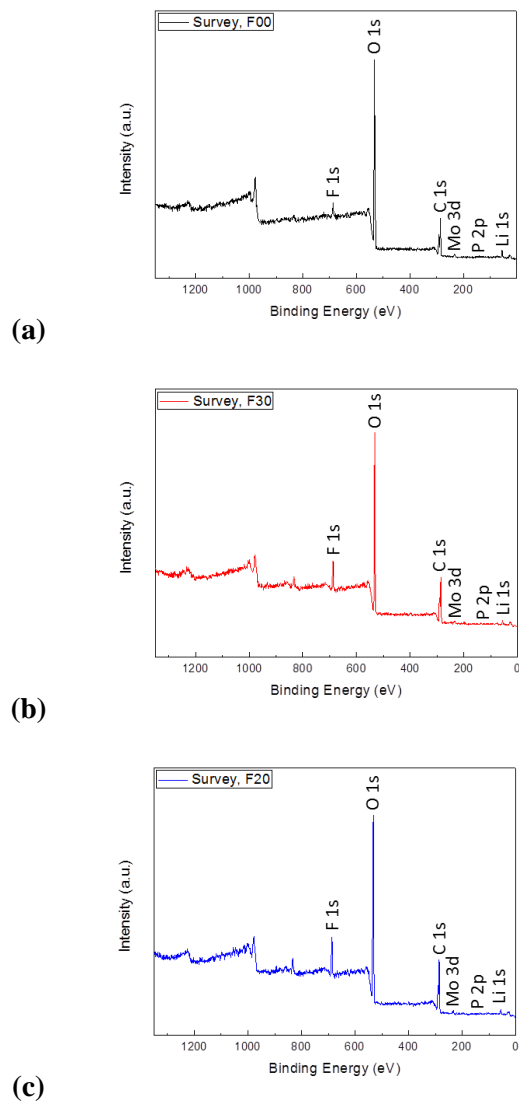
Figure 3.9. Survey XPS spectra of the cycled a-MoO$_2$ electrodes in (a) F00, (b) F30, and (c) F20 electrolytes after 50 cycles. The various elements of interest, Mo 3d, F 1s, O 1s, C 1s, Li 1s, and P 2p, were employed to obtain chemical information about the surface films.
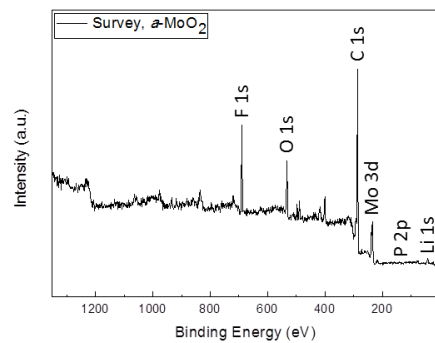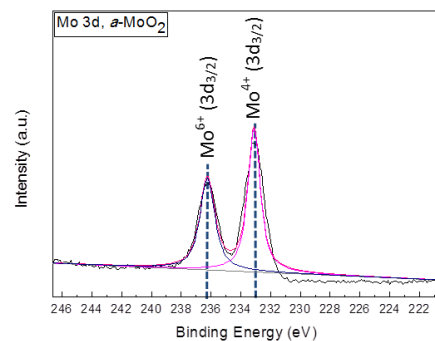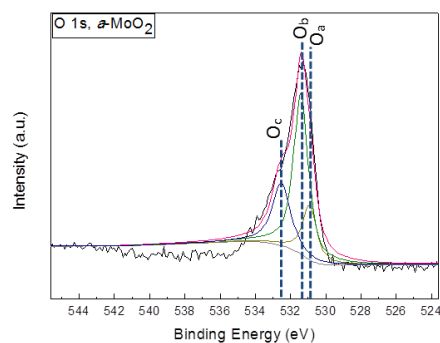
Figure 3.10. (a) Survey XPS spectra of the as-fabricated *a*-MoO₂ electrode. High-resolution XPS spectra of (b) Mo 3d and (c) O 1s for as-fabricated electrode before conducting galvanostatic battery cycling.

(a)

(b)
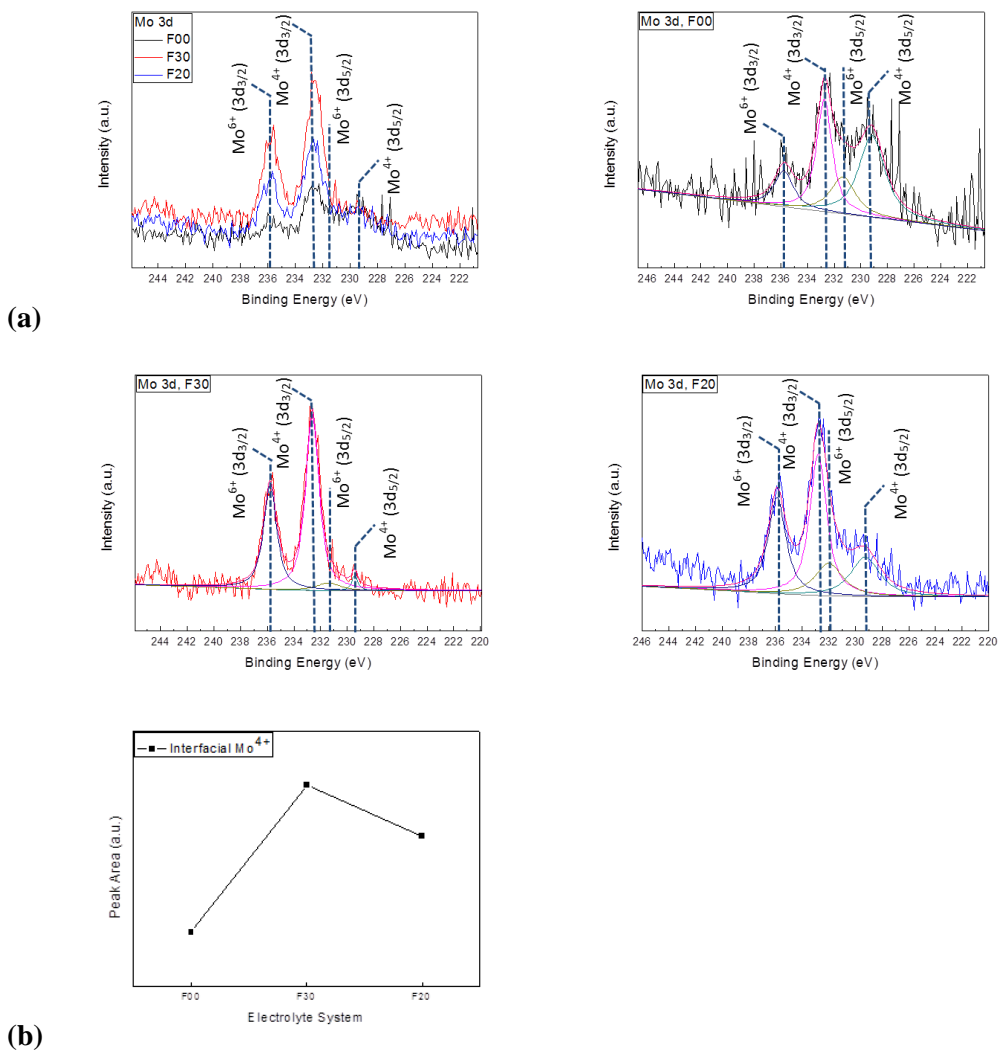
Figure 3.11. (a) High-resolution XPS spectra of Mo 3d for cycled electrodes in different electrolyte systems after 50 cycles. Combined and the individual deconvoluted spectra of cycled electrodes in different electrolytes with navy dashed lines marked for characteristic electronic state of molybdenum. (b) Comparison of interfacial Mo^{4+} content in each electrolyte system on the basis of quantitative analysis of the spectra, which reflects the relative surface film thickness.
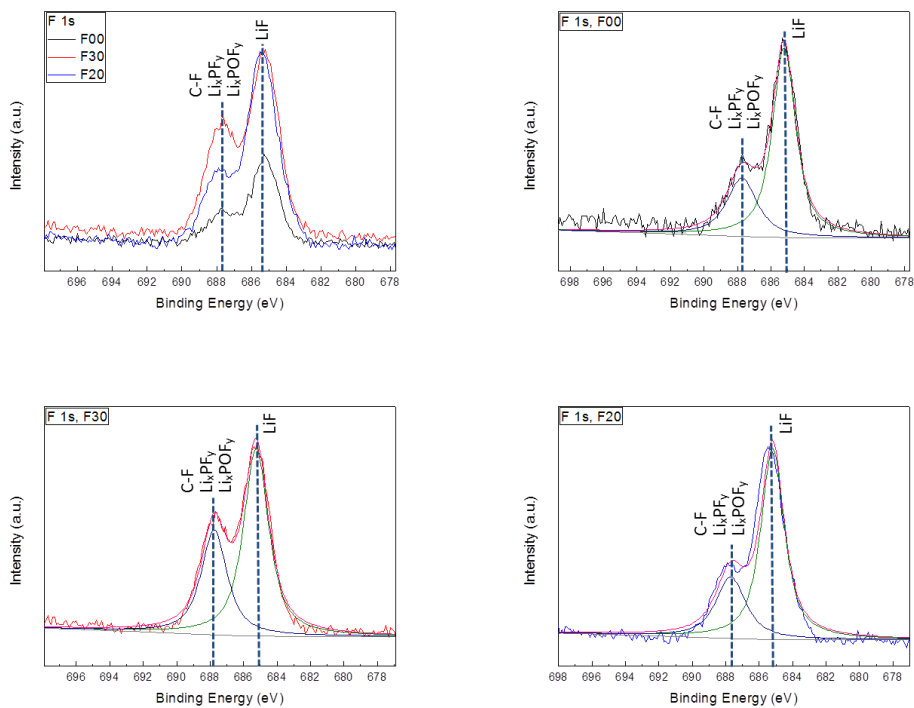
Figure 3.12. High-resolution XPS spectra of F 1s for cycled electrodes in different electrolyte systems after 50 cycles. Combined and the individual deconvoulted spectra of cycled electrodes in different electrolytes with navy dashed lines marked for interfacial LiF and other fluorine-containing materials.
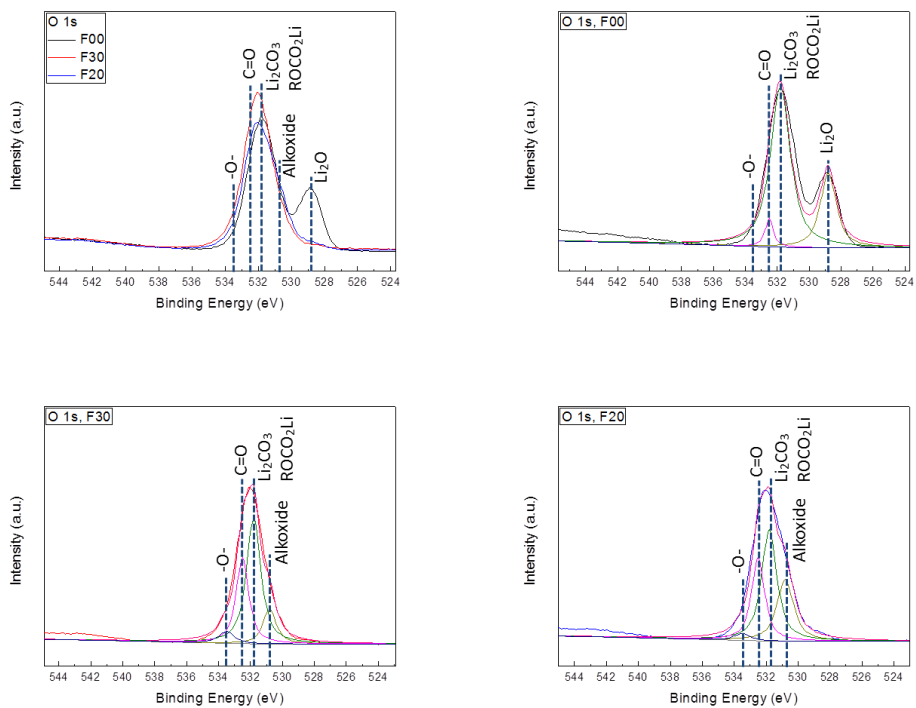
Figure 3.13. High-resolution XPS spectra of O 1s for cycled electrodes in different electrolyte systems after 50 cycles. Combined and the individual deconvoulted spectra of cycled electrodes in different electrolytes with navy dashed lines marked for oxygen-containing characteristic materials.
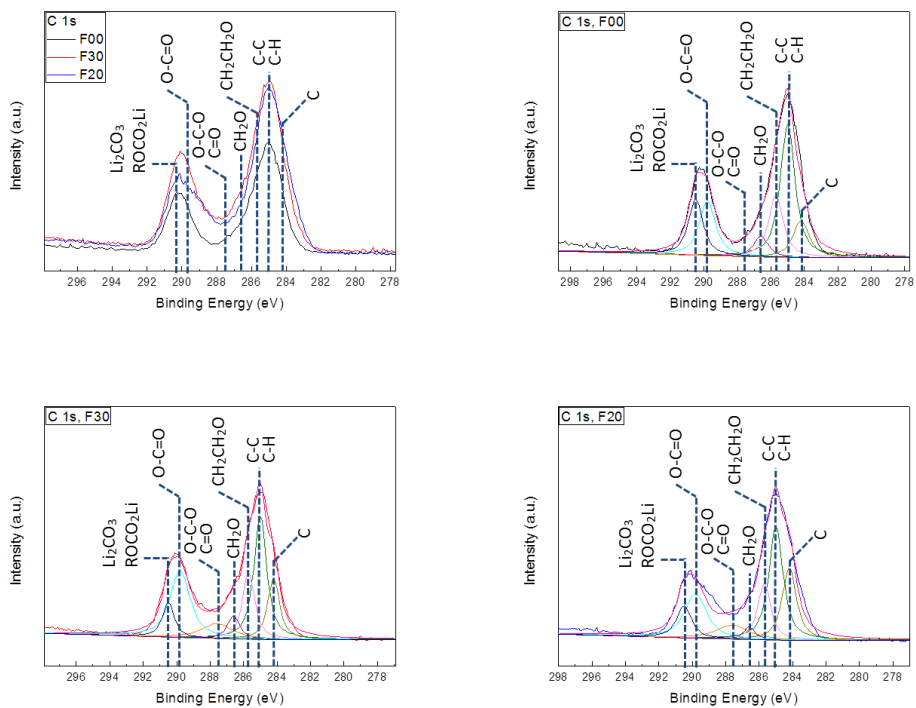
Figure 3.14. High-resolution XPS spectra of C 1s for cycled electrodes in different electrolyte systems after 50 cycles. Combined and the individual deconvoulted spectra of cycled electrodes in different electrolytes with navy dashed lines marked for carbon-containing characteristic materials.
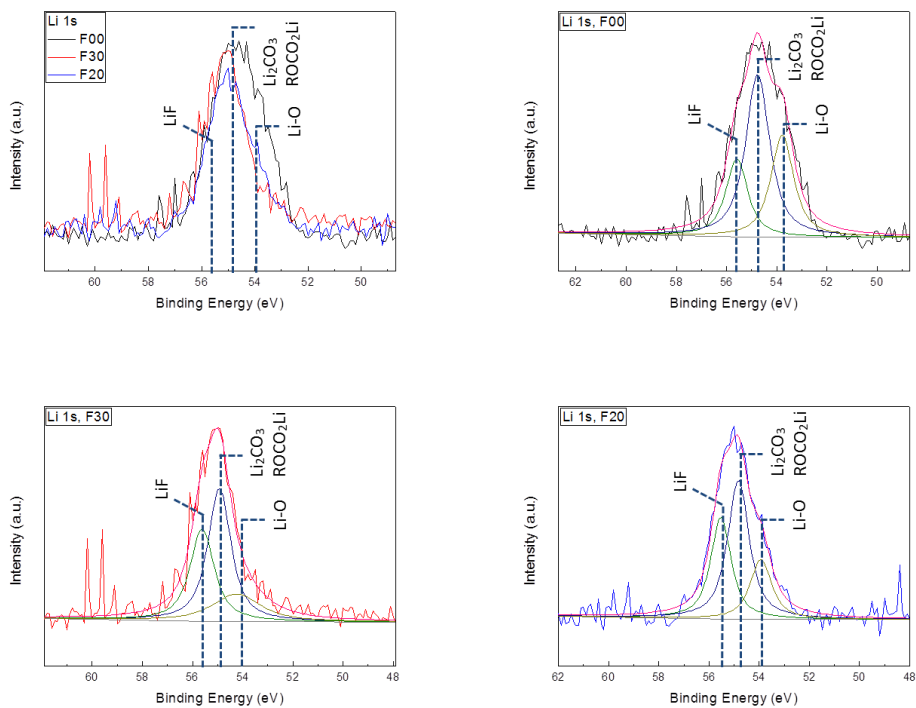
Figure 3.15. High-resolution XPS spectra of Li 1s for cycled electrodes in different electrolyte systems after 50 cycles. Combined and the individual deconvoulted spectra of cycled electrodes in different electrolytes with navy dashed lines marked for lithium-containing materials.
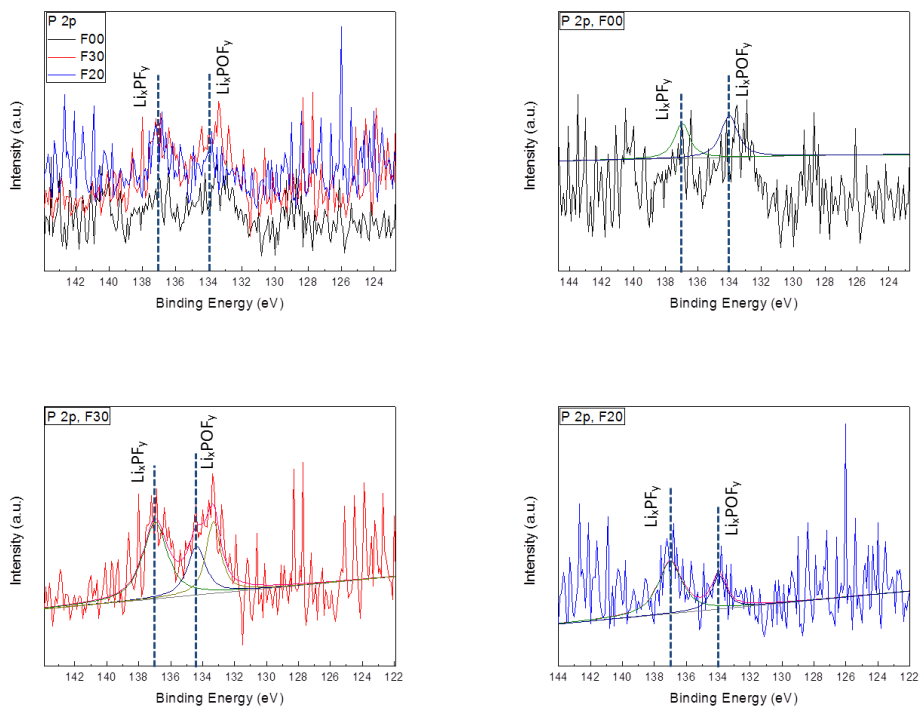
Figure 3.16. High-resolution XPS spectra of P 2p for cycled electrodes in different electrolyte systems after 50 cycles. Combined and the individual deconvoulted spectra of cycled electrodes in different electrolytes with navy dashed lines marked for phosphorus-containing materials.

3.4. SEI Formation Mechanism

Degradation in electrochemical battery performance caused by SEI stability issue can be summarized in several factors; the consumption of electrolyte and lithium ions during continuous SEI formation, the electrically insulating nature of the SEI weakening the electrical contact between the current collector and negative electrode, the long lithium ion diffusion distance through the thickened SEI, and electrode material degradation caused by mechanical stress from the SEI.[70] The formation and control of a stable SEI is critical for realizing promotion in cycleability for electrode materials subject to large volume changes including transition metal oxides.

The microscopic and spectroscopic characterizations of the a-MoO$_2$ negative electrodes enabled us to identify important aspects of their surface chemistry. The chemical structure and property of surface films formed in three different electrolytes, as discussed so far, provide an idea about different SEI formation behavior in regard of the film thickness, mechanical and electrochemical stability, and lithium ion conductivity. In this section, SEI formation mechanism of a-MoO$_2$ negative electrode in FEC-free and FEC-containing systems is proposed based on the findings of electrochemical behavior and surface characterization studied in advance.

3.4.1. EC-derived SEI

EC reduction was the primary process for the surface chemistry in F00 electrolyte. EC-

derived SEI (Figure 3.17(a)) exhibits a mosaic-type film with heterogeneous distribution of EC-reduced products as reported by many groups including E. Peled's group.[56] In the scheme, the various lithium carbonate organics and inorganics were notated as alphabets from A to E. The surface film composed of EC-reduced soluble products generates microvoids inside the film (red arrow in Figure 3.17(a)), which is a vacant space that allow easy and continuous electrolyte penetration. The continuous SEI formation mechanism from the first lithiation is illustrated as well. The transition metal oxides including MoO_2 accompany approximately 100% of massive volume change upon de-/lithiation.[23] Then the initially formed inflexible lithium carbonate-based surface film can be damaged or cracked during the delithiation because of the volume change of underlying active material. As a result, the electrolyte permeates through the damaged SEI and reacts with the exposed electrode that leads to additional side reaction to form extra films. The repeated side reaction results in surface film thickening, which is responsible for severe impedance rise and capacity fading. In short, EC-derived SEI was thick, mechanically and electrochemically unstable, and highly resistive for lithium ion transport. Although the conventional transition metal oxide nanostructures guarantee a fine level of cycle performance, there is an absolute opportunity to improve the battery performance by modifying the surface film property and its formation mechanism upon repetitive cycling.

3.4.2. FEC-derived SEI

Meanwhile the preferential reduction of FEC and following VC polymerization were the primary processes in F30 electrolyte to form compact and dense FEC-derived SEI (Figure 3.17(b)). The main FEC-reduced and/or VC-polymerized products were polycarbonates and insoluble inorganic LiF. The nature of these solid products could guarantee high flexibility, impermeability, and lithium ion conductivity of the FEC-derived SEI. Investigation of SEI formation procedure indicates that the film can endure volume change of the a-MoO$_2$ without a critical film deformation. A high quality FEC-derived SEI is supported by mechanical stability upon volume change of active material and electrochemical stability to electrolyte permeation that can inhibit the film damage and thickening. Moreover a thin and lithium ion conductive FEC-derived SEI makes it possible for easy and fast lithium ion transfer across the film. It can lower the overpotential and charge transfer impedance for better cycleability.[42] The superior property of FEC-derived SEI and its formation mechanism could explain a better passivation and enhanced electrochemical battery performance of a-MoO$_2$ negative electrode. To summarize, FEC-derived SEI, in the case of total replacement of EC with FEC, was thin, mechanically and electrochemically stable, and highly ion conductive. The involvement of FEC in surface chemistry provides an exciting ability for high quality interface control. It is able to conclude that FEC as a co-solvent successfully modified the surface chemistry of a-MoO$_2$ negative electrode at room temperature.

3.4.3. EC-/FEC-co-derived SEI

The examination of F20 electrolyte resulted in the competition between EC and FEC in the surface film formation. A competition of chemical reaction between FEC (or VC obtained from reductive decomposition of FEC) and EC continuously occurs at the first and subsequent lithiation processes,[42] and thereby the film contained both VC-polymerized and EC-reduced products. As depicted in Figure 3.17(c), EC-/FEC-co-derived SEI might be blended with both of the EC- and FEC-reduced products but a bit of difference in the population of them. The inner and outer regions of surface film are expected to be dominantly composed of FEC-reduced and EC-reduced products, respectively; named as FEC-derived inner SEI and EC-derived outer SEI. This idea is based on the two facts; the formation of preliminary FEC-derived SEI due to preferential reduction of FEC and similar passivating ability to FEC-derived SEI observed in surface characterization. These factors imply the passivating materials close to active surface must be rich in FEC-reduced products. FEC is the most reactive component in the electrolyte since it has higher reduction potential than that of EC or DEC. Therefore the FEC-reduced products are more likely to be formed in advance and occupy relatively inner part of total surface film. EC-reduced products are formed after the reduction of FEC and they may accumulate in the film to take up relatively outer part of the SEI. This explanation seems consistent with surface characterization of FEC-derived and EC-/FEC-co-derived SEI. O 1s high-resolution XPS spectra of EC-/FEC-co-derived SEI resembled those of FEC-derived SEI, not the EC-derived SEI. The O 1s spectra reflected passivating ability of each film on surface oxidation by verifying the presence of Li_2O and/or O_2 in surface species. Hence we could infer that the chemical structure of FEC-derived and EC-/FEC-co-derived SEI are alike at the active material surface meaning that

passivating materials close to surface are rich in FEC-reduced products rather than EC-reduced products. Thus despite of the severe damage on frail EC-derived outer SEI caused by the large volume change of underlying a-MoO$_2$, robust FEC-derived inner SEI still serves as an effective and firm passivation film. It leads to the enhancement in battery performance of F20 electrolyte compared to that of F00 electrolyte. However degraded battery performance compared to that of F30 electrolyte is unavoidable since EC-derived outer SEI and EC-reduced products inside FEC-derived inner SEI degrade the quality of the total surface film. The FEC impact on EC-/FEC-co-derived SEI is weakened due to its lower concentration coupled with the presence of EC, but does not negate all of the benefits of FEC-containing system.[31] To sum up, EC-/FEC-co-derived SEI exhibited median surface film properties as well as the battery performance that depended on FEC concentration.

Since both of the EC and FEC solvents must be reduced as the electrodes are fully lithiated, EC-/FEC-co-derived SEI is obviously the one-phase structure, not the two-phase or layer-by-layer structure of solid products. To roughly confirm the progress of reduced products formation upon cycling, FT-IR spectra variation upon several selected cycles was investigated. Such investigation may give an idea about the complicated chemical structure of EC-/FEC-co-derived SEI in terms of relative quantitative observation of the reduced products inside the total film. After only one galvanostatic cycle, the pronounced peaks of FEC-reduced products were observed (Figure 3.18(a)), as in the case of previous FEC-derived SEI spectra. But after the second cycle (Figure 3.18(b)), the pronounced peaks around 2800 cm^{-1} and 1600 ~ 600 cm^{-1} that correspond to EC-reduced products were intensified. After 20 cycles (Figure 3.18(c)), the spectral

features converged to those of previous EC-/FEC-co-derived SEI. Such a change in spectra reflects the blended structure of EC- and FEC-reduced products. And it also implies the preliminary FEC-derived film exists throughout entire cycling and firmly passivates the active material surface. Then it might provide more logics on the fact that FEC-reduced products are preliminarily formed and occupy relatively inner position (at the 1st cycle) followed by EC-reduced products accumulation in comparatively outer position of the total film (from the 2nd cycle). It seems that the participation of EC-reduced products dominantly takes place in the film thickening procedure, which arises from the reaction between electrolyte and newly exposed electrode surface. However, the direct proof in population of the reduced products in the structure of EC-/FEC-co-derived SEI cannot be identified at this point, and further analysis with appropriate approach is required.
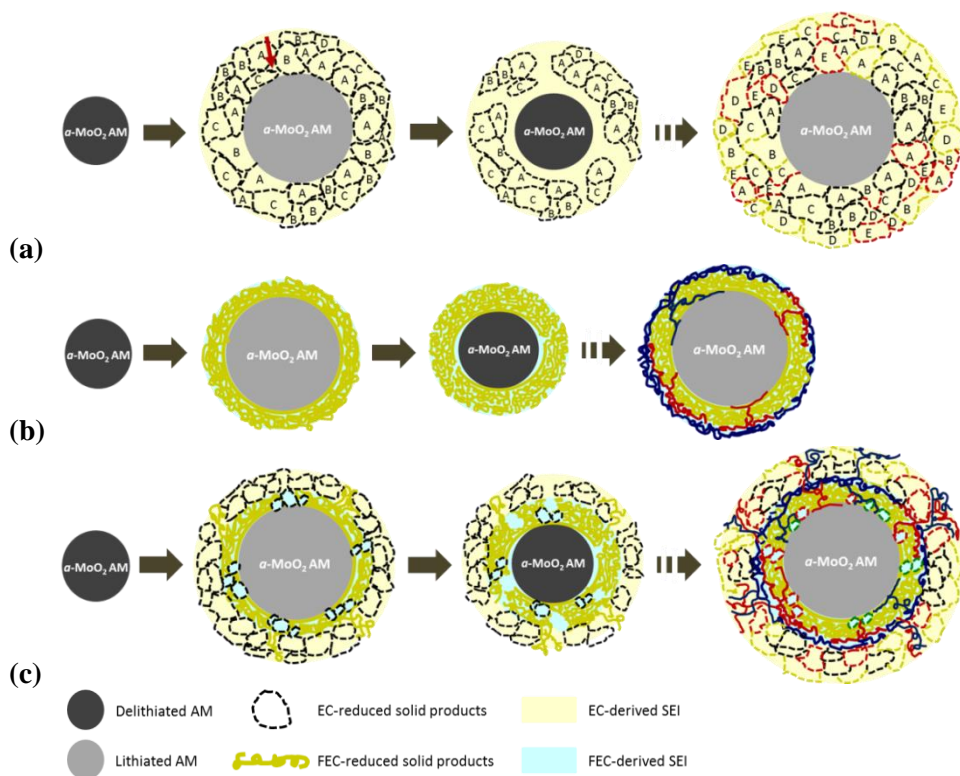
Figure 3.17. SEI formation mechanism for the first de-/lithiation and the following lithiation processes for (a) EC-derived, (b) FEC-derived, and (c) EC-/FEC-co-derived SEI, respectively. The first two figures represent as-fabricated active material (AM) and the surface films formed after the first lithiation. The next two figures represent the first delithiation that leads to film damage and subsequent lithiation that forms additional solid products to recover exposed active material. The repetitive de-/lithiation processes are omitted for all cases. The changed colors of irregular figures (EC-reduced products) and winding lines (FEC-reduced products) indicate continuous growth of the films. Red ones for the first reformation of solid products refer to both EC- and FEC-reduced products. The continued solid products formations are expressed by green color for EC-reduced products and blue color for FEC-reduced products, respectively.

(a)

(b)

(c)
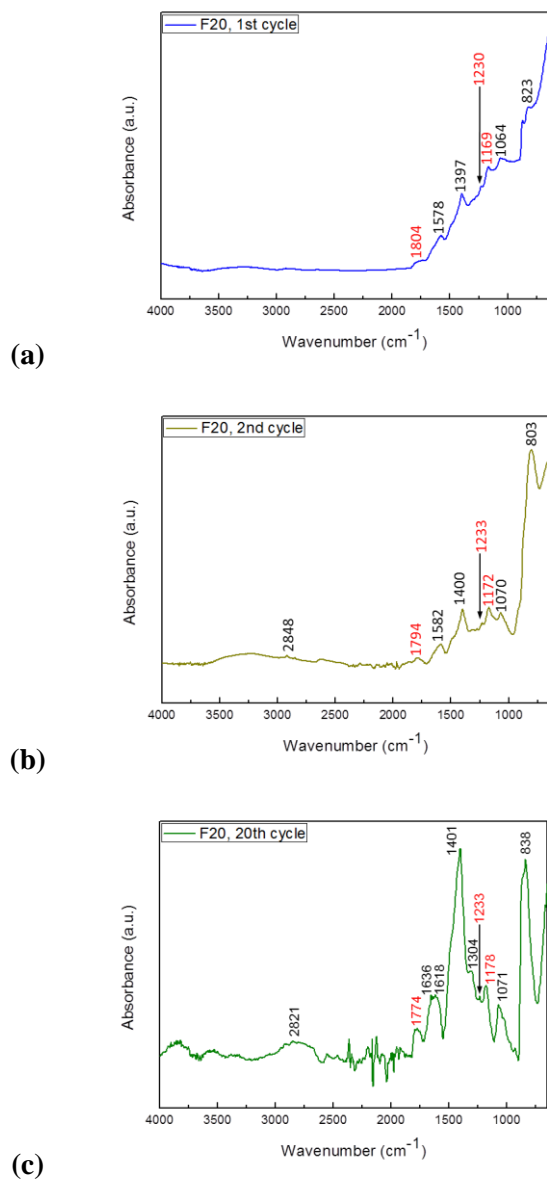
Figure 3.18. ATR FT-IR spectra of a-MoO$_2$ electrodes cycled in F20 electrolyte after the (a) 1st cycle, (b) 2nd cycle, and (c) 20th cycle. The analysis conditions were as same as the other surface characterizations.

4. Conclusions

In this research, we investigated the effect of FEC as an alternative co-solvent on the electrochemical battery performance and surface chemistry of a-MoO$_2$ lithium-ion secondary battery negative electrode. The promotion of battery performance was due to the positive impacts of FEC in the high quality surface film derived by modified surface reaction of a-MoO$_2$.

The cycling performance of the cells in FEC-containing electrolyte system was improved compared to that in FEC-free system. FEC-containing system exhibited high coulombic efficiency around 99% and prolonged discharge capacity retention as a function of FEC concentration up to approximately 7% after 50 cycles. The enhanced electrochemical performance was attributed to superior SEI properties caused by FEC addition.

Microscopic and spectroscopic investigations proved the superior SEI formation in presence of FEC in regard of the ion conductivity, mechanical and electrochemical stability, and the thickness. FE-SEM images showed the fine morphology of SEI without collapse of the electrode structure in all the electrolyte systems. To gain an insight into the chemical structure and electrochemical properties of each surface film, spectroscopic investigations were conducted. EC-derived SEI exhibited drastic increase in its impedance for interfacial lithium ion transfer reaction. It was rich in soluble and inflexible lithium carbonate organics as confirmed in FT-IR and XPS spectra. And it was the thickest film as informed from XPS spectra. In a word, a highly resistive, frail, and

thick EC-derived SEI was formed by EC reduction. On the other hand, when FEC is involved, the lower impedance could be achieved. The flexible polycarbonates and insoluble LiF were rich in the surface species of FEC-containing system. Lastly the FEC-derived SEI was thinner than any other SEI discussed herein. To summarize, when EC is totally replaced by FEC, a highly conductive, flexible, robust and thin FEC-derived SEI was formed. EC-/FEC-co-derived SEI showed combined characteristics of EC-derived and FEC-derived SEIs. These properties originated from the characteristic surface species formed in each electrolyte system. Thus it is able to conclude that FEC successfully modified the surface chemistry of a-MoO$_2$ negative electrode at room temperature.

Ultimately, based on the findings in electrochemical battery performance and surface characterization, we developed SEI formation mechanisms that can explain the correlation between battery performance and surface chemistry of electrode material. After the very initial formation of surface films, the inflexible lithium carbonate-based EC-derived SEI can be broken down during following delithiation since it cannot endure a massive volume change of a-MoO$_2$. The repetitive side reaction between electrolyte and newly exposed active surface leads to severe film thickening. Meanwhile polycarbonate-based FEC-derived SEI can retain its structure upon cycling due to its mechanical and electrochemical stability. Then the film thickening is hindered, which makes it able to lower the overpotential and charge transfer impedance. EC-/FEC-co-derived SEI is blended in both of the EC- and FEC-reduced products with a bit of difference in population of those solid products; named as FEC-derived inner SEI and EC-derived outer SEI. Although the FEC impact on the film is weakened due to the

degradation of total film quality by EC-reduced products, the benefits of FEC-reduced products are still realized. We expect that the SEI formation mechanism could help in better understanding of the FEC effect in prolonged cycle performance and able to be applied in other lithium-ion secondary battery negative electrodes as well.

References

[1] R. E. Smalley, *MRS Bulletin*, **30** (2005).

[2] G. A. Nazri, G. Pistoia, *Lithium Batteries: Science and Technology*, Kluwer Academic/Plenum: Boston (2004).

[3] Y. Liang, S. Yang, Z. Yi, X. Lei, J. Sun, Y. Zhou, *Mat. Sci. Eng. B*, **121**, 152 (2005).

[4] M. Wagemaker, W. J. H. Borghols, F. M. Mulder, *J. Am. Chem. Soc.*, **129**, 4323 (2007).

[5] L. C. Yang, Q. S. Gao, Y. H. Zhang, Y. Tang, Y. P. Wu, *Electrochem. Commun.*, **10**, 118 (2008).

[6] X. Ji, P. S. Herle, Y. Rho, L. F. Nazar, *Chem. Mater.*, **19**, 374 (2007).

[7] Y. Shi, B. Guo, S. A. Corr, Q. Shi, Y. S. Hu, K. R. Heier, L. Chen, R. Seshadri, G. D. Stucky, *Nano Letters*, **9**, 4215 (2009).

[8] Q. Gao, L. Yang, X. Lu, J. Mao, Y. Zhang, P. Wu, Y. Tang, *J. Mater. Chem.*, **20**, 2807 (2010).

[9] Z. Wang, J. S. Chen, T. Zhu, S. Madhavi, X. W. Lou, *Chem. Comm.*, **46**, 6906 (2010).

[10] Y. Liang, S. Yang, Z. Yi, J. Sun, Y. Zhou, *Mater. Chem. Phys.*, **93**, 395 (2005).

[11] P. L. Taberna, S. Mitra, P. Poizot, P. Simon, J. M. Tarascon, *Nat. Mater.*, **5**, 567 (2006).

[12] D. Larcher, D. Bonnin, R. Cortes, I. Rivals, L. Personnaz, J. M. Tarascon, *J. Electrochem. Soc.*, **150**, A1643 (2003).

[13] J. Chen, L. Xu, W. Li, X. Gou, *Adv. Mater.*, **17**, 582 (2005).

[14] M. V. Reddy, T. Yu, C. H. Sow, Z. X. Shen, C. T. Lim, G. V. S. Rao, B. V. R. Chowdari, *Adv. Funct. Mater.*, **17**, 2792 (2007).

[15] A. Manthiram, C. Tsang, *J. Electrochem. Soc.*, **143**, L143 (1996).

[16] Z. W. Fu, F. Huang, Y. Q. Chu, Y. Zhang, Q. Z. Qin, *J. Electrochem. Soc.*, **150**, A776 (2003).

[17] T. A. Kim, J. H. Kim, M. G. Kim, S. M. Oh, *J. Electrochem. Soc.*, **150**, A985 (2003).

[18] H. Furukawa, M. Hibino, I. Honma, *J. Electrochem. Soc.*, **151**, A527 (2004).

[19] H. T. Fang, M. Liu, D. W. Wang, T. Sun, D. S. Guan, F. Li, J. Zhou, T. K. Sham, H. M. Cheng, *Nanotechnology*, **20**, 1 (2009).

[20] W. J. H. Borghols, D. Lutzenkirchen-Hecht, U. Haake, W. Chan, U. Lafont, E. M. Kelder, E. R. H. van Eck, A. P. M. Kentgens, F. M. Mulder, M. Wagemaker, *J. Electrochem. Soc.*, **157**, A582 (2010).

[21] M. Armand, J. –M. Tarascon, *Nature*, **451**, 652 (2008).

[22] J. Kim, M. K. Chung, B. H. Ka, J. H. Ku, S. Park, J. H. Ryu, S. M. Oh, *J. Electrochem. Soc.*, **157**, A412 (2010).

[23] P. Poizot, S. Laruelle, S. Grugeon, L. Dupont, J. M. Tarascon, *Nature*, **407**, 496 (2000).

[24] D. Aurbach, Y. Gofer, *Nonaqueous Electrochemistry*, Marcel Dekker: New York (1999).

[25] J. Vetter, P. Novak, M. R. Wagner, C. Veit, K. –C. Moller, J. O. Besenhard, M. Winter, M. Wohlfahrt-Mehrens, C. Vogler, A. Hammouche, *J. Power Sources*, **147**, 269 (2005).

[26] K. Xu, *Chem. Rev.*, **104**, 4303 (2004).

[27] K. Naoi, M. Mori, M. Inoue, T. Wakabayashi, K. Yamauchi, *J. Electrochem. Soc.*, **147**, 813 (2000).

[28] D. Aurbach, K. Gamolsky, B. Markovsky, Y. Gofer, M. Schmidt, U. Heider, *Electrochim. Acta*, **47**, 1423 (2002).

[29] S. S. Zhang, *J. Power Sources*, **162**, 1379 (2006).

[30] R. McMillan, H. Slegr, Z. X. Shu, W. D. Wang, *J. Power Sources*, **81**, 20 (1999).

[31] Y. Lin, K. C. Klavetter, P. R. Abel, N. C. Davy, J. L. Snider, A. Heller, C. B. Mullins, *Chem. Commun.*, **48**, 7268 (2012).

[32] C. Tsang, A. Dananjay, J. Kim, A. Manthiram, *Inorg. Chem.*, **35**, 504 (1996).

[33] F. Xia, X. Hu, Y. Sun, W. Luo, Y. Huang, *Nanoscale*, **4**, 4707 (2012).

[34] J. H. Ku, Y. S. Jung, K. T. Lee, C. H. Kim, S. M. Oh, *J. Electrochem. Soc.*, **156**, A688 (2009).

[35] A. Debart, L. Dupont, P. Poizot, J. B. Leriche, J. M. Tarascon, *J. Electrochem. Soc.*, **148**, A1266 (2001).

[36] D. Larcher, G. Sudant, J. B. Leriche, Y. Chabre, J. M. Tarascon, *J. Electrochem. Soc.*, **149**, A234 (2002).

[37] P. Poizot, S. Laruelle, S. Grugeon, J. M. Tarascon, *J. Electrochem. Soc.*, **149**, A1212 (2002).

[38] J. H. Ku, J. H. Ryu, S. H. Kim, O. H. Han, S. M. Oh, *Adv. Funct. Mater.*, **22**, 3658 (2012).

[39] M. N. Obrovac, L. J. Krause, *J. Electrochem. Soc.*, **154**, A103 (2007).

[40] C. K. Chan, R. Ruffo, S. S. Hong, R. A. Huggins, Y. Cui, *J. Power Sources*, **189**, 34 (2009).

[41] S. Laruelle, S. Grugeon, P. Poizot, M. Dolle, L. Dupont, J. M. Tarascon, *J. Electrochem. Soc.*, **149**, A627 (2002).

[42] V. Etacheri, O. Haik, Y. Goffer, G. A. Roberts, I. C. Stefan, R. Fasching, D. Aurbach, *Langmuir*, **28**, 965 (2012).

[43] L. Chen, K. Wang, X. Xie, J. Xie, *J. Power Sources*, **174**, 538 (2007).

[44] I. A. Profatilova, S. S. Kim, N. S. Choi, *Electrochim. Acta*, **54**, 4445 (2009).

[45] S. S. Zhang, K. Xu, T. R. Jow, *Electrochim. Acta*, **51**, 1636 (2006).

[46] L. E. Ouatani, R. Dedryvere, C. Siret, P. Biensan, D. Gonbeau, *J. Electrochem. Soc.*, **156**, A468 (2009).

[47] H. Park, T. Yoon, J. Mun, J. H. Ryu, J. J. Kim, S. M. Oh, *J. Electrochem. Soc.*, **160**, A1539 (2013).

[48] Y. Wang, S. Nakamura, M. Ue, P. B. Balbuena, *J. Am. Chem. Soc.*, **123**, 11708 (2001).

[49] S. H. Lee, Y. H. Kim, R. Deshpande, P. A. Parilla, E. Whitney, D. T. Gillaspie, K. M. Jones, A. H. Mahan, S. B. Zhang, A. C. Dillon, *Adv. Mater.*, **20**, 3627 (2008).

[50] H. Nakai, T. Kubota, A. Kita, A. Kawashima, *J. Electrochem. Soc.*, **158**, A798 (2011).

[51] N. S. Choi, K. H. Yew, K. Y. Lee, M. Sung, H. Kim, S. S. Kim, *J. Power Sources*, **161**, 1254 (2006).

[52] B. Liu, B. Li, S. Guan, *Electrochem. Solid-State Lett.*, **15**, A77 (2012).

[53] K. Tasaki, A. Goldberg, J. –J. Lian, M. Walker, A. Timmons, S. J. Harris, *J. Electrochem. Soc.*, **156**, A1019 (2009).

[54] S. Leroy, F. Blanchard, R. Dedryvere, H. Martinez, B. Carre, D. Lemordant, D.

Gonbeau, *Surf. Interface Anal.*, **37**, 773 (2005).

[55] S. Park, J. H. Ryu, S. M. Oh, *J. Korean Electrochem. Soc.*, **15**, 19 (2012).

[56] E. Peled, D. Golodnitsky, G. Ardel, *J. Electrochem. Soc.*, **144**, L208 (1997).

[57] M. Chen, X. Wang, Y. H. Yu, Z. L. Pei, X. D. Bai, C. Sun, R. F. Huang, L. S. Wen, *Appl. Surf. Sci.*, **158**, 134 (2000).

[58] P. –T. Hsieh, Y. –C. Chen, K. –S. Kao, C. –M. Wang, *Appl. Phys. A*, **90**, 317 (2008).

[59] B. Scrosati, J. Garche, *J. Power Sources*, **195**, 2419 (2010).

[60] K. Miushima, P. C. Jones, P. J. Wiseman, J. B. Goodenough, *Mat. Res. Bull.*, **15**, 783 (1980).

[61] A. S. Arisco, P. Bruce, B. Scrosati, J. M. Tarascon, W. V. Schalkwijk, *Nat. Mater.*, **4**, 366 (2005).

[62] J. –M. Tarascon, M. Armand, *Nature*, **414**, 359 (2001).

[63] X. Zhao, M. Cao, B. Liu, Y. Tian, C. Hu, *J. Mater. Chem.*, **22**, 13334 (2012).

[64] L. Yang, L. Liu, Y. Zhu, X. Wang, Y. Wu, *J. Mater. Chem.*, **22**, 13148 (2012).

[65] G. Girishkumar, B. McCloskey, A. C. Luntz, S. Swanson, W. Wilcke, *J. Phys. Chem. Lett.*, **1**, 2193 (2010).

[66] P. B. Balbuena, Y. Wang, *Lithium-Ion Batteries: Solid-Electrolyte Interphase*, Imperial College Press: London (2004).

[67] H. Groult, T. Nakajima, L. Perrigaud, Y. Ohzawa, H. Yashiro, S. Komaba, N. Kumagai, *J. Fluorine Chem.*, **126**, 1111 (2005).

[68] M. Gaberscek, R. Dominko, J. Jamnik, *J. Power Sources*, **174**, 944 (2007).

[69] I. Choi, M. J. Lee, S. M. Oh, J. J. Kim, *Electrochim. Acta*, **85**, 369 (2012).

[70] H. Wu, G. Chan, J. W. Choi, I. Ryu, Y. Yao, M. T. McDowell, S. W. Lee, A. Jackson,

Y. Yang, L. Hu, Y. Cui, *Nature Nanotechnology*, **7**, 310 (2012).

[71] Y. Sun, X. Hu, W. Luo, Y. Huang, *ACS Nano*, **5**, 7100 (2011).

Appendix

A.1. Effect of Polymerizable Monomers

The polymerizable monomers are another type of SEI former additive. They include vinylene carbonate (VC), vinyl ethylene carbonate (VEC), vinyl acetate (VA), and so forth. The common structural feature of these additives is that they contain a double bond between carbons. This molecular structure makes them able to undergo electrochemically induced polymerization; radical anion termination by solvent molecules to form insoluble and stable solid products as preliminary SEI nuclei. However, L. E. Ouatani and coworkers found out that the polymerization of these monomers depends on the systems as a function of electrode nature. It implied that not every SEI former additives are able to modify the surface reaction such as polymerization of additives at the electrode surface.

FEC reductive decomposition mechanism brought about VC and HF generation. VC served as polymerizable additive and HF served as acidic impurity which were responsible for formation of polymeric species and transformation of SEI components, respectively, for a successful modification in surface chemistry of a-MoO$_2$. Then it was desirable to confirm rather polymerizable additives or monomers alone could lead to battery performance promotion with notable change in surface chemistry of a-MoO$_2$. The electrochemical battery performance of nano-sized a-MoO$_2$ was estimated in electrolytes of 1.3 M LiPF$_6$/EC:DEC = 30:70 vol% containing 1 wt% of VC, VEC, and VA.
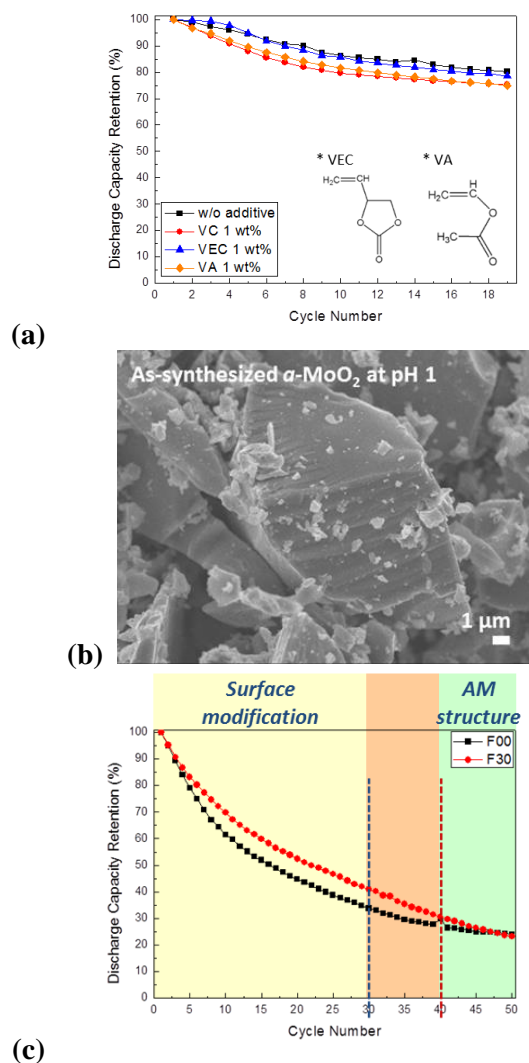
Discharge capacity retention of a-MoO$_2$ in additive-free and polymerizable monomer-containing electrolytes is demonstrated in Figure 1(a). After 20 cycles, the cycleability of polymerizable monomer-containing electrolytes was similar to or even poor than that of additive-free electrolyte. It was conclusive that polymerizable monomers did not help in improving cycle performance and it was possibly due to the failure in surface chemistry modification of nano-sized a-MoO$_2$ negative electrodes at room temperature. The combination of SEI former additive and electrode material is another obvious determinant factor for battery performance improvement as well as successful surface chemistry modification.

A.2. Effect of a-MoO$_2$ Particle Size

The micron-sized a-MoO$_2$ particles were obtained from pH 1 of reaction mixture, which was composed of Mo^{6+} precursor solution and reducing agent solution. The particles were irregular in shape with angulated platelets sized about 1 ~ 10 µm, and the surface of larger particles was covered with some tiny particles as shown in Figure 1(b). A change in pH of reaction mixture did not affect either the crystallinity or the oxidation state of MoO$_2$ (XRD data not shown here).

The electrochemical battery performance of micron-sized a-MoO$_2$ negative electrodes was investigated by comparing EC-based and FEC-based electrolyte system (Figure 1(c)). Micron-sized a-MoO$_2$ showed drastic decrease in cycleability compared to that of nano-sized electrode in both of EC-based and FEC-based cells. It was contributed to the effect

of particle size. The bulk electrode materials show severe capacity fading in common due to the collapse of electrode structure, e.g. particle pulverization, and accelerated lithium ion consumption resulting irreversible capacity loss. FEC-based F30 electrolyte exhibited the maximum enhancement of battery performance for nano-sized a-MoO$_2$ negative electrodes. However, it did not induce any improvement in prolonged cycleability for micron-sized a-MoO$_2$. In fact, the capacity retention of F30 system was absolutely higher than that of F00 system until 30 cycles. It was contributed to the dominant surface chemistry modification derived by FEC. However a rapid and drastic decrease in cycle performance of F30 system after 30 cycles was observed. It may be indicative of two opposing effects occurring after 30 cycles; surface chemistry modification and collapse of electrode structure. The capacity retention of two different systems reflected that the superior surface film property derived by FEC became negligible due to the collapse of electrode structure. The electrochemical behavior of micron-sized a-MoO$_2$ in presence of FEC implied that there must be an underlying relationship between surface chemistry modification and electrode structure. It was conclusive that the involvement of FEC did not cause the positive impacts for micron-sized a-MoO$_2$ negative electrodes at room temperature.

(a)

(b)

(c)

Figure 1. (a) Discharge capacity retention of nano-sized a-MoO$_2$ in polymerizable monomer-containing electrolytes for 20 cycles. Chemical structures of VEC and VA are illustrated in the inset of (a). (b) FE-SEM image of as-synthesized particles obtained from pH 1 of reaction mixture and (c) discharge capacity retention of micron-sized a-MoO$_2$ for 50 cycles.

초 록

리튬이온 이차전지는 우수한 에너지 저장 성능을 기반으로 에너지 저장 시스템 구현에 있어 가장 유망한 전기화학적 소자이다. 리튬이온 이차전지의 성공에도 불구하고 새로운 전극 소재의 개발과 안정적 계면 제어를 통한 리튬이온 이차전지의 용량, 에너지 및 출력 밀도 향상을 위해 많은 연구들이 지속적으로 수행되어왔다. 다양한 전극 물질 후보군 중에서 몰리브데늄 이산화물은 상당히 낮은 전기적 저항과 높은 열적, 화학적 안정성과 같은 우수한 특성에 기인하여 리튬이온 이차전지의 음극 소재 중 하나로 검토되어 왔다. 그러나 다른 전극 소재들과 마찬가지로 반복적인 정전압 사이클 과정 이후 몰리브데늄 이산화물 전극 표면에도 표면피막이 형성된다. 표면피막의 형성은 리튬이온 이차전지 시스템에서 필연적인 부반응으로서 전지 성능의 퇴화를 유발하기 때문에 전지의 장기 구동 성능과 밀접한 연관을 갖는다. 따라서 몰리브데늄 이산화물 전극 기반의 리튬이온 이차전지에서도 높은 이온 전도도, 물리적, 전기화학적 안정성, 그리고 얇은 두께를 갖는 표면피막을 형성하기 위해 피막에 대한 정확한 분석과 제어가 요구된다.

본 연구에서는 비정질 몰리브데늄 이산화물 나노 입자 음극의 전기화학적 전지 성능 및 표면피막 형성 메커니즘에 있어 대표적인 표면피막 형성 첨가제인 플루오르에틸렌 카보네이트의 긍정적 효과를 관찰하였다. 다양한 함량의 플루오르에틸렌 카보네이트를 전해질의 대체 조용매로 첨가하여 비정질 몰리

브데늄 이산화물 전극의 전기화학적 거동을 설명할 수 있는 서로 다른 표면 피막 형성 메커니즘을 규명하고자 하였다. 50 사이클 구동 이후 플루오르에틸 렌 카보네이트 농도에 따라 용량 보유값이 최대 약 7%까지 증가하였다. 플루 오르에틸렌 카보네이트를 함유한 전해질 시스템에서 비정질 몰리브데늄 이산 화물의 전기화학적 성능을 설명하기 위해 전기화학 임피던스 분광법, 필드 방 사 주사 전자 현미경법, 푸리에 변환 적외 분광법, 그리고 X선 광전자 분광법 을 사용하여 계면화학 반응을 분석하였다. 전극 표면에서 플루오르에틸렌 카 보네이트의 성공적인 환원 분해 결과로 높은 이온 전도성을 가지고 물리적, 전기화학적으로 안정하며 얇은 표면피막을 형성할 수 있었다. 이러한 피막 특 성은 폴리카보네이트와 리튬 플루오라이드가 풍부한 플루오르에틸렌 카보네 이트 환원 물질로부터 기인하였다. 연구 결과들을 토대로 플루오르에틸렌 카 보네이트의 존재 유무에 따른 에틸렌 카보네이트, 플루오르에틸렌 카보네이트, 그리고 에틸렌 카보네이트와 플루오르에틸렌 카보네이트에서 공동으로 유도 되는 각각의 표면피막 성질을 규명하고 이들의 형성 메커니즘을 고안하였다. 본 논문에서 제시하는 표면피막 형성 메커니즘 규명은 일반적인 리튬이온 이 차전지 음극에서의 계면화학 반응을 개선하는데 효과적인 대체 조용매로서의 플루오르에틸렌 카보네이트 효과를 이해하는데 도움이 될 수 있다. 현재까지 파악된 바에 의하면 플루오르에틸렌 카보네이트를 사용한 비정질 몰리브데늄 이산화물 음극의 계면화학 메커니즘 규명은 본 연구에서 처음 수행하였다.

감사의 글

대학원에 진학하여 석사 연구생으로서 학업을 이어간 것이 어느덧 2년이 지났습니다. 어느 누구에게나 그렇듯 다사다난한 일들이 있었지만 이제 그 모든 시간을 성공적으로 마무리하고 또 한 번의 도전을 앞두고 있습니다. 그 동안 물심양면으로 저를 격려해주시고 응원해주셨던 여러분들께 이 기회를 빌어 감사한 마음을 조금이나마 표현하고자 합니다.

가장 먼저 늘 저의 가장 든든한 후원자이자 버팀목인 아버지, 어머니, 그리고 올 해 취업에 성공한 동생 미정이. 가족들의 따뜻한 관심과 응원 덕에 지금의 자리까지 무사히 올 수 있었습니다. 가장 가까이 함께하는 가족이지만 생각만큼 많이 소중함과 고마움을 직접 표현하지는 못해왔네요. 학부 졸업 기념 동영상부터 늘 조금 더 믿고 기다려주세요 라는 말을 많이 한 것 같아 아쉽고 죄송한 마음이 크지만 이 모든 과정이 제게 반드시 필요한 도약의 단계가 되도록, 그리고 그 과정의 끝에 행복한 가족의 일원으로서 든든한 아들, 오빠의 모습 보일 수 있도록 꾸준히 노력하겠습니다. 늘 온 마음을 담아 감사하고 지금까지처럼 그리고 지금보다 더욱 건강하고 행복한 우리 가족이 되었으면 좋겠어요.

제 학위 과정 간 저의 학업적 성과는 물론 여타 다양한 부분에 있어 아낌없는 조언과 지도를 해주신 김재정 교수님께도 진심 어린 감사의 말씀을 드립니다. 교수님의 일관된 지도를 통해 소기의 성과와 많은 경험, 추억을 가지

고 학위 과정을 마칠 수 있게 되었습니다. 이제 잠시 교수님의 품을 떠나 다른 목표에 도전하고자 합니다. 그 동안의 소중한 가르침 잊지 않고 더 당당하고 한 걸음 도약한 제자의 모습으로 다시 인사드릴 수 있도록 늘 노력하겠습니다.

연구실에서 2년 동안 함께 지내며 저의 부족한 면을 채워주신 여러 선배, 동료들에게도 감사의 말씀을 드리고 싶습니다. 김수길 교수님, 권오중 교수님. 아주 먼 인생 후배, 연구실 후배이지만 학회장이나 실험실에서 후배라는 인연으로 관심 가져 주시고 따뜻한 말 한마디 건네주셔서 감사합니다. 저의 영원한 사수 인수 형. 형이 잘 가르쳐 주신 덕에 형이 떠난 뒤에도 많이 생각해보고 적극적으로 찾아서 해결하는 힘을 기를 수 있었어요. 때로 황당할 수도 있는 저의 부족한 견해를 끝까지 들어주신 것 진심으로 본받고 싶은 모습으로 간직하고 있습니다. 지금은 직장인이 된 민정이. 좋은 서포트 해주는 후배가 되었어야 했는데 부족했던 것 같아서 미안... 우리 소수 정예 배터리 팀 언제 회식 한번 하자. 또 여러 졸업하신 선배들, 상현이 형, 승욱이 형, 경주 누나. 함께 한 시간이, 추억이 많지는 않았지만 많이 배우고 즐거운 시간이었습니다. 자주 연락도 못 드리고 하지만 계신 곳에서 잘 지내고 계시리라 믿고 저도 좋은 모습으로 나중에 다시 인사 드리겠습니다.

태호 형. 좋은 멘토가 왜 필요한지 형 덕에 절실히 깨닫게 되었습니다. 형의 손길이 닿지 않았다면 지금의 논문이 완성될 수 없었을 거에요. 지금 이 글을 쓰는 순간 이후에도 종종 형을 귀찮게 하겠지만... 늘 웃는 모습으로 제

SOS에 응답해 주셔서 감사합니다. 명준이 형. 형의 많은 관심과 독려가 저로 하여금 좀 더 많은 생각을 하고 조금이라도 현재 수준에서 한 단계 업그레이드 시켜보고자 하는 노력이 가능하도록 해주었습니다. 형들에게 도움 받은 만큼 저도 나중에 형들에게 도움이 될 수 있는 후배가 되도록 최선을 다하겠습니다. 학부 선배이자 연구실 선배이신 강욱이 형. 제가 좀 더 살갑게 다가갔어야 하는데 못 그런 것 같아 죄송합니다. 야구하실 때 몸 건강히 하시고 성대라인으로 종종 연락 드리겠습니다. 기호 형. 형과 같이 수업 듣고 양꼬치 먹을 때 너무도 즐거웠습니다. 제가 아주 살가운 편은 못되어서 형하고 더 가까워지지 못한 것 같아 아쉽지만 이 인연으로 계속 잘 지내서 나중에 쌍둥이도 같이 보고 싶네요. 광환이, 승회. 동갑내기 친구로 잘 지내줘서 너무 고마워. 두 친구 덕에 쉽고 빠르게 잘 적응할 수 있었어. 광환이는 방장하느라 이제 더 바쁠 것 같은데 워낙 성실하고 꼼꼼히 지내는 너니까 잘 지내리라 믿어. 승회도 지금처럼 똑똑하고 유쾌한 모습 언제 어디에서든 계속 기대할게. 회철이, 명호. 형인 후배를 만나서 하고 싶은 이야기도 못한 부분도 꽤 있을 것 같은데 이 자리를 빌어 그런 부분이 있었다면 미안하고... 회철이 2년 동안 훌륭한 동료로, 샤프한 선배로 있어줘서 고마워. 나의 마지막, 그리고 유일한 팀 멤버 명호. 시간이 지날 수록 명호랑 점점 더 많은 이야기 나누고 시간을 공유할 수 있어서 다행이야. 내가 새로운 도전을 선택했지만 앞으로도 같은 연구분야를 갖은 동료로서 잘 지내자. 안나 누나. 저랑 들은 수업 때문에 첫 학기부터 고생하셨죠? 바쁘신 와중에도 항상 웃으면서 만나주셔서 늘 감

사했습니다. 학위과정 잘 진행되시길 바랄게요. 유석, 윤지. 내 성격이 사소한 부분에서 오히려 아무렇게나 넘어가지 않는 부분이 있어서 아마 나랑 지내는 게 쉽지만은 않았을 것 같아. 식상하지만 나름 너희를 위해서 한 말이었으니 너무 서운하게 생각하지 않았으면 좋겠고 너희도 각자 분야에서 좋은 성과 얻고 더욱 잘 지내길 바란다. 신입생인 성경, 승연, 영근. 지금 이 글을 쓰는 시점이 심지어 첫 출근도 아직 안 했지만... 어떤 일을 하든지 쉽고 만만한 일은 없다고들 하니까 여러분이 선택한 일, 선택한 공간인 만큼 즐기면서 지낼 수 있기를 바래요. 송이 누나. 제가 입학할 때부터 함께했는데 벌써 2년이라는 시간이 지났네요. 입사동기(?)로서 더 잘 지냈어야 했는데 부족했던 것 같아 죄송해요. 항상 감사했고 몸 안 좋으신 것 쾌차하셔서 얼른 맛있는 음식 마음껏 드실 수 있길 바래요. 짧지만 같이 시간을 보낸 인천대 친구들, 만수, 재승이, 현석이, 현준이, 강훈이. 이제 다들 각자의 자리를 잡고 지내게 되었구나. 앞으로도 종종 연락하고 얼굴 볼 수 있길 바라고 학부생일 때부터 열심히 지내는 너희의 모습에서 많이 배웠었다. 마지막으로 내 동기들, 혁진이, 상원이. 몇 번 우리끼리 얘기하면서 한 말이지만 너희 없이 실험실 생활할 수 있었을까 하는 마음이 늘 떠나지 않는다. 허당 매력으로 나의 보호 본능을 깨우는 혁진이. 입사 축하하고 새로운 자리에서 그 자리를 빛내는 친구되길 바래. 주위 사람을 유쾌하게 만들어주는 그 힘, 어디에서나 잘 통할 것이라 믿어. 자신을 무척 사랑하는 상원이. 너의 당차고 에너지 넘치는 모습 언제나 보기 좋았어. 덕분에 옆에 있는 나도 많이 기분 전환되곤 했다. 이제 상원이

랑 나는 또 다른 목표를 가지고 새로운 출발선에 섰는데 우리 둘 다 좋은 결실 얻을 수 있길 바래보자.

이제 정리를 해야 할 것 같아서 길게는 못 쓰겠지만... 학위 기간 동안 같은 분야에 있는 친구로서 내게 가장 큰 버팀목이 되어준 미루. 네 존재가 나한테는 무척 고마웠어. 앞으로도 우리 우정 계속 갈 수 있길 바란다! 나만의 삼총사 동완, 동현! 동완이 회사 열심히 잘 다니고 무릎 조심해. 시간이 있을지 모르겠지만 겨울이라고 정신 없이 보드만 타지 말고. 동현이 시험 준비 잘 해서 우리 동업자가 되기로 한 약속 꼭 지키자. 자랑스러운 모교의 동아리와 학과 친구, 선후배님들! 종종 학교로 돌아가 여러분의 기를 받은 덕에 이 순간을 맞이할 수 있었습니다. 각자 자리에서 열심히 나아가면서 때때로 지난 추억도 함께 떠올리고 새로운 추억 역시 많이 쌓을 수 있었으면 좋겠어요. 이제 다들 바빠서 자주는 못 보지만 늘 그리운 친구들! 각자의 자리에서 빛나는 우리가 될 수 있으면 좋겠다. 한 명, 한 명 언급은 못했지만 그 간 많은 응원과 격려해주신 모든 여러분께 다시 한 번 진심으로 감사의 마음을 전하고 싶습니다. 그 격려 절대 잊지 않고 한 발, 한 발 나아가 더 도약하는 모습 보여드릴 수 있도록 하겠습니다. 진심으로 감사합니다.

2014년 2월

박 종 우 올림